ISSN 1075-7015, Geology of Ore Deposits, 2008, Vol. 50, No. 5, pp. 362–390. © Pleiades Publishing, Ltd., 2008.
Original Russian Text © N.A. Goryachev, O.V. Vikent'eva, N.S. Bortnikov, V.Yu. Prokof'ev, V.A. Alpatov, V.V. Golub, 2008, published in Geologiya Rudnykh Mestorozhdenii, 2008, Vol. 50, No. 5, pp. 414–444.

The World-Class Natalka Gold Deposit, Northeast Russia: REE Patterns, Fluid Inclusions, Stable Oxygen Isotopes, and Formation Conditions of Ore

N. A. Goryachev[a], O. V. Vikent'eva[b], N. S. Bortnikov[b], V. Yu. Prokof'ev[b], V. A. Alpatov[c], and V. V. Golub[a]

[a]*Northeast Interdisciplinary Research Institute, Far East Division, Russian Academy of Sciences, Portovaya ul. 16, Magadan, 685000 Russia*

[b]*Institute of Geology of Ore Deposits, Petrography, Mineralogy, and Geochemistry, Russian Academy of Sciences, Staromonetnyi per. 35, Moscow, 119017 Russia*

[c]*Institute of Geology of Diamond and Noble Metal Deposits, Siberian Branch, Russian Academy of Sciences, pr. Lenina 39, Yakutsk, 677891 Russia*

Received December 15, 2007

Abstract—REE patterns of hydrothermally altered rocks, fluid inclusions, and stable oxygen isotopes of quartz were studied at the Natalka gold deposit. Metasomatic rocks formed under decompression reveal gradual depletion in LREE and HREE relative to siltstone of the protolith. The HREE patterns of metasomatic rocks formed under decompression are uniform; an insignificant removal of LREE can be noted. The progressive extraction of REE with increasing alteration of rocks could have been due to the effect of magmatogenic or meteoric fluid. Because a Ce anomaly is absent, the participation of oxidized meteoric water was limited. The inverse correlation between the total REE content and the Eu anomaly value in altered rocks indicates a substantial role of magmatogenic fluid. The REE patterns of altered rocks formed under compression show that the role of metamorphic fluid was not great. All metasomatic rocks are enriched in LREE, so that the enrichment of fluid in LREE as well may be suggested. Three fluid compositions were captured as fluid inclusions: (1) H_2O–CO_2–NaCl–$MgCl_2$ with a salinity of 1.0–4.9 wt % NaCl equiv, (2) CO_2–CH_4, and (3) H_2O–NaCl–$MgCl_2$ with a salinity of 7.0–5.6 wt % NaCl equiv. Compositions (1) and (2) coexisted in the mineral-forming system at 250–350°C and 1.1–2.4 kbar as products of phase separation under conditions of decreasing *P* and *T*. The interaction of this fluid with host rocks resulted in the formation of extensive halos of beresitized rocks with sulfide disseminations. The precipitation of arsenopyrite and pyrite led to the substantial depletion of mineral-forming fluid in H_2S and destabilization of the $Au(HS)^{2-}$ complex. The fluid with the third composition arose due to the boiling of the H_2O–CO_2–CH_4–NaCl–$MgCl_2$ liquid and was responsible for metasomatic alteration of host rocks. The late mineral assemblages were deposited from this fluid at the initial stage of ore formation. The high methane concentrations in the ore-forming fluid were likely caused by interaction of hydrothermal ore-bearing solutions with carbonaceous host rocks. The $\delta^{18}O$ values of quartz from quartz–scheelite–pyrite–arsenopyrite and sulfide–sulfosalt mineral assemblages vary from +11.6 to +14.1‰ and +11.2 to +13.5‰, respectively. The parental fluids of the early and late mineral assemblages probably were derived from a magmatic source and were characterized by $\delta^{18}O_{H_2O}$ = +6.3 to +8.8‰ at 350°C and +3.6 to +5.9‰ at 280°C, respectively. The narrow interval of oxygen isotopic compositions shows that this source was homogeneous. The data obtained allow us to suggest that the deposit formation was related to magmatic activity, including the direct supply of ore components from a magma chamber and mobilization of these components in the processes of dehydration and decarbonation during contact and regional metamorphism.

DOI: 10.1134/S1075701508050024

INTRODUCTION

The Natalka gold deposit was discovered in 1942 by E.P. Mashko. In 1944–2004, the deposit was the object of underground mining and intense scientific research. This is a world-class superlarge deposit (Grigorov, 2006). According to Lashkov et al. (2000) and Struzhkov et al. (2006), more than 90 t of gold have been mined out from primary ore and 105 t from the Omchak placer, related to the Natalka deposit. The follow-up exploration of the deposit in 2004–2007 resulted in the estimation of resources at 1760 t with a Au grade of 1.7 g/t (Grigorov, 2006).

This deposit is a typical example of orogenic deposits localized in collision belts composed of volcanosedimentary and terrigenous rocks metamorphosed under conditions of greenschist facies (Goldfarb et al., 2005).

Corresponding author: O.V. Vikent'eva. E-mail: viken@igem.ru

The origin of large and superlarge deposits is important because, in the estimation of D.V. Rundqvist, about 80% of mineral resources are mined from deposits of these classes. The main constituents of conceptual genetic models simulating hydrothermal ore-forming systems responsible for the formation of large and superlarge deposits include (1) the geodynamic setting of deposits and the history of regional geological evolution; (2) the tectonic structure of deposits, particularly, the paths of hydrothermal fluid migration into the zone of ore deposition; (3) the stages of hydrothermal system development and its duration; (4) the sources of ore-bearing fluids and metals; (5) the composition of ore-forming fluids, conditions of fluid migration, and speciation of metals therein; and (6) the conditions, causes, and mechanisms of ore deposition. The elucidation of the composition and nature of ore-forming fluids is not only of academic interest but also serves as a guide for choice of a geological exploration strategy.

The origin of orogenic gold deposits hosted in terrigenous clayey and clayey–carbonate rocks and black shales remains a matter of debate. Various opinions on their origin—from hydrothermal sedimentary to postmagmatic or metamorphic—have been set forth (Sidorov and Tomson, 2000; Buryak et al., 1990; Kurbanov et al., 1994; Hodgson et al., 1993; Kerrich et al., 2000). No universal view on the genesis of gold–quartz and stringer–disseminated deposits exists; one group of researchers refers them to different genetic types, whereas another regards these deposits as genetically cognate (Bierlein and Maher, 2001). The composition of mineral-forming fluids and their sources are subjects of hot discussion (Bortnikov, 2006; Kerrich, 1990; Groves et al., 2003; Goldfarb et al., 2005; Bortnikov and Prokof'ev, 2007). Goldfarb et al. (1989) stated a hypothesis on a crucial role of metamorphism in the formation of ore-forming fluids. A convective meteoric model of the formation of gold deposits in the Northern Cordilleras was developed by Nesbitt and Muchlenbachs (1989). A concept suggesting a leading role of postmagmatic fluid mixed in the ore-forming system with metamorphic fluid was proposed in (Bortnikov, 1995; Bortnikov et al., 1993, 1996, 1997).

To ascertain the origin and composition of the fluid responsible for the formation of the Natalka deposit, we focused on the distribution of REE and other trace elements in metasomatic rocks, fluid inclusions in quartz from quartz–pyrite and quartz–pyrite–arsenopyrite Au-bearing veins and veinlets, and the oxygen isotopic composition of quartz.

GEOLOGY

The Natalka deposit is situated in the Omchak goldfield, which also includes the Omchak and Pavlik deposits. The goldfield is localized on the southwestern limb of the Ayan-Yuryakh Anticlinorium, which extends in the northwestern direction at the southeastern flank of the collision-related Yana–Kolyma Orogenic Belt (*Geodynamics*…, 2006) and is composed of Upper Permian sedimentary and volcanosedimentary rocks more than 2.5 km in total thickness and Triassic siltstone.

The structure of the Omchak goldfield was formed at the collision and postcollision stages, accompanied by emplacement of various igneous complexes. Intrusive rocks occur as numerous small stocklike bodies and a few relatively large granite and granodiorite plutons up to 300 km^2 in area (Goncharov et al., 2002) at flanks of the Ayan-Yuryakh Anticlinorium. In the central part of this anticlinorium, close to the Natalka deposit, the large plutons give way to small stocks and dike suites (Fig. 1). The plutons are composed of diverse rocks from gabbro and pyroxenite to leucogranite and granite porphyry. Spessartite, diorite, and granite porphyry dikes, as well as dikes of intrusive rhyolite, are widespread. Taken together, they are regarded as an intrusive framework of the goldfield (Goncharov et al., 2002). The large plutons are subdivided into heterogeneous, often multiphase bodies (the Intrigan–Peresypkino and Necha plutons) and relatively homogeneous bodies (the Tenkechan and Mirazh plutons). As a rule, the small intrusive bodies are heterogeneous as well, with gradual transitions between diorite, quartz diorite, and granodiorite. Remnants of Cretaceous volcanic rocks (Goryachev, 2003) are accompanied by late ore mineralization at gold deposits (Sidorov et al., 2003).

Dikes—spessartite, diorite porphyry, granite porphyry, and intrusive rhyolite—are an important factor in localization of ore mineralization. The ore-bearing dikes group in small swarms concentrating in the central portion of the goldfield and at its eastern and northern flanks. The dikes are oriented along the strike of country rocks and are often located in fault zones. The thickness of dikes varies from 1–2 to 6–8 m, occasionally reaching 15–20 m (Goncharov et al., 2002). Dikes of different compositions are commonly separated in space. Rare intersections indicate that spessartite and diorite porphyry are the oldest; they are cut by altered granite porphyry. The results of isotopic dating of plutons and dikes testify to at least two stages of magmatic activity in the Omchak goldfield. The granite of the Tenkechan pluton is dated at 156–143 Ma, and the Necha domes, at 101–83 Ma (Firsov, 1964); dikes of premineral spessartite and diorite porphyry are 159–130 Ma in age and postmineral spessartite and rhyolite are not older than 100 Ma (Firsov, 1967). These estimates do not contradict the $^{40}Ar/^{39}Ar$ age of spessartite dikes and wall-rock metasomatic alteration (137–135 Ma) at the Natalka deposit (Newberry et al., 2000). According to geochronological and geochemical data (Goncharov et al., 2002), the plutonic rocks in the goldfield belong to the premineral Late Jurassic–Early Cretaceous diorite–granodiorite series and the postmineral Cretaceous granodiorite–granite and Late Cretaceous granite–rhyolite series (Goncharov et al., 2002). The

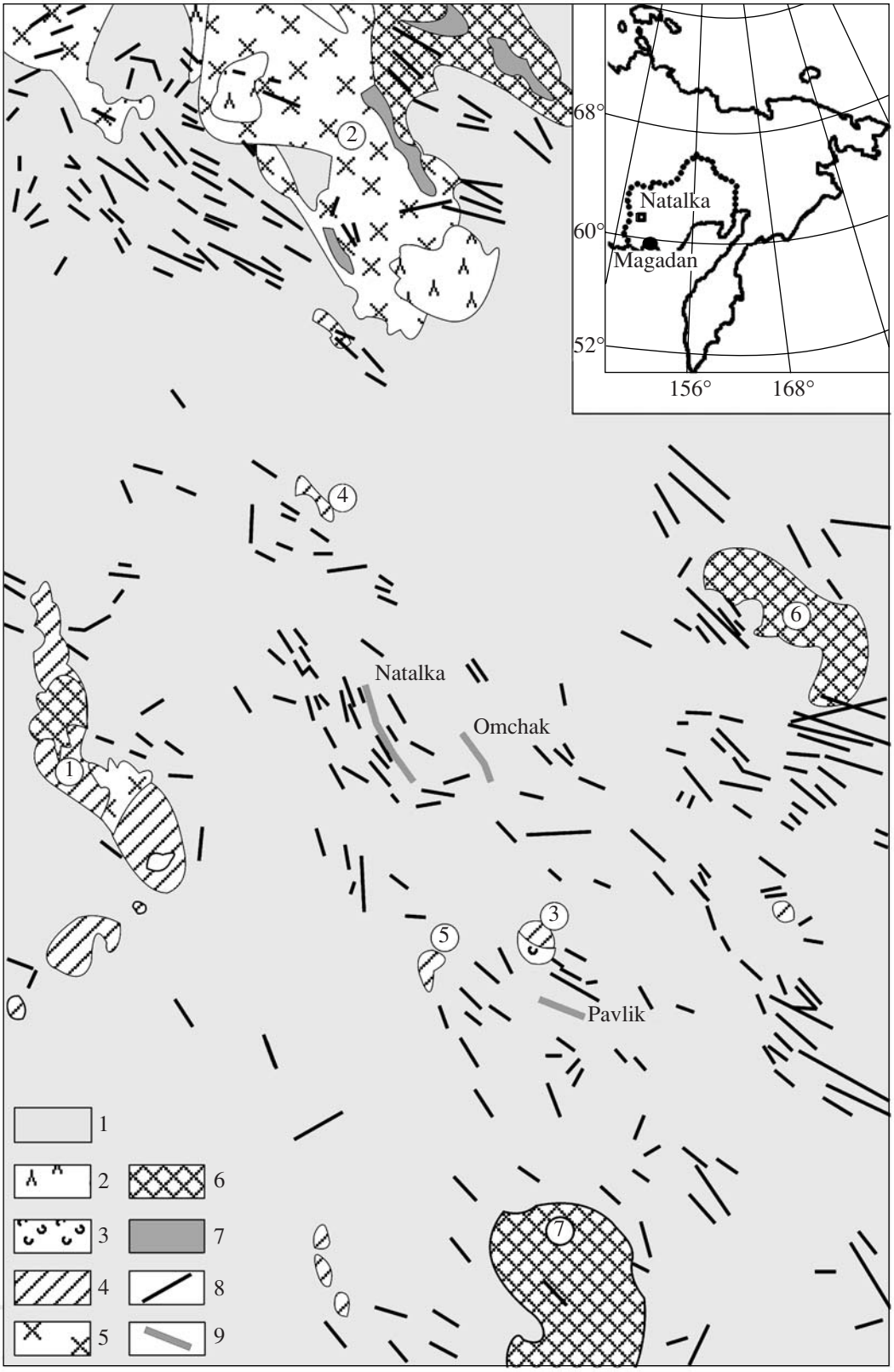

Fig. 1. Location of intrusive bodies and ore deposits in the Omchak ore cluster, after Goncharov et al. (2002). (1) Permian and Triassic sedimentary and volcanosedimentary rocks, (2) Lower Cretaceous volcanic rocks, (3) Cretaceous rhyolite, (4) gabbro and diorite, (5) granodiorite, (6) granite, (7) leucogranite, (8) dikes, (9) ore deposits. Granitoid plutons (numerals in circles): (1) Intrigan–Peresypkino, (2) Necha, (3) Vanin, (4) Butuz; (5) Vilka, (6) Mirazh, (7) Tengkechan.

gold mineralization is related in space and time to the early diorite–granodiorite plutonic series (Newberry et al., 2000), whereas Sn and Mo occurrences are associated with the Cretaceous plutonic series (Goncharov et al., 2002; Mirgorodskaya et al., 2005).

The Natalka deposit is localized in the zone affected by the large NW-trending Ten'ka Fault Zone (Goncharov et al., 2002). At the surface, this zone is expressed in the Main and Northwestern faults, which bound a wedge-shaped block that hosts the main ore mineralization (Kalinin et al., 1992). The simple symmetric Natalka Syncline is a structural element of the second order relative to the Ten'ka Anticline (Kalinin et al., 1992). Its length is about 4.5 km and its width is 2.5 km. This morphology is close to a brachysyncline. Most likely, the doming controlled the formation of the block structure of the goldfield, consisting of the Central, Glukhar Creek, and Natalka Creek blocks, differing in abundance of dikes, intensity of deformation, and gold mineralization. Numerous premineral spessartite and granite porphyry dikes are known in the goldfield; granitoid plutons differing in age are located at the flanks (at a distance of 10–20 km) (Goncharov et al., 2002).

According to geophysical data, a large hidden granitoid pluton is located to the northeast of the deposit in the root zone of a group of ore-controlling faults (Mezhov and Khasanov, 2001; Khasanov et al., 2001). The occurrence of this intrusive body is validated by physical properties of ore-bearing sedimentary rocks in deep holes, the enrichment of these rocks in pyrrhotite and As-bearing pyrite with depth (Sharafutdinov and Khasanov, 2006; Tyukova and Voroshin, 2007), and an increase in the amount of visible gold and its grain size in this direction (Struzhkov et al., 2006).

The Natalka deposit is localized in Permian sedimentary and volcanosedimentary rocks subdivided into the Pioner, Atkan, and Omchak formations (Mezhov, 2000; Goncharov et al., 2002; Struzhkov et al., 2006) (Fig. 2). The orebodies are hosted largely in the Atkan Formation, composed of siltstone with an admixture of medium and coarse clastic volcaniclastic rocks, which have been referred to in various publications as tuffaceous slate, pebble-bearing siltstone, "ryabchik" (hazel-grouse) tuffaceous siltstone, or diamictite (Pristavko et al., 2000; Stepanov, 2001). The orebodies are traced along large faults in under- and overlying rocks for as far as 200 m from the Atkan Formation (Struzhkov et al., 2006). The gold mineralization is controlled by longitudinal and oblique tectonic zones that complicate the southwestern limb of the Natalka Syncline, including the master Main and Northwestern faults.

The more than 120 orebodies known at the deposit are clustered into southwestern, northeastern, and central suites (Pristavko et al., 2000) that make up a mineralized zone more than 7 km in extent. At the northwestern flank, the width of this zone is 100–150 m; it increases up to 400 m in the central segment and over 1000 m farther to the southeast. In cross section, the ore zone is fan-shaped and diverges up the dip.

In structure and morphology, the orebodies (ore zones) are subdivided into stringer–metasomatic, stringer–vein, and vein types and mineralized shear zones (Mezhov, 2000). The stringer–metasomatic ore zones (8/23, 6/9, 7, 13, etc.), with a highest Au grade of 10–15 g/t, are characterized by numerous high-grade pockets and lenses distributed irregularly. The stringer–vein orebodies (3, 3/62, 6/25) contain up to 15–20 g/t Au near the contact between the Atkan and Omchak formations. The vein-type orebodies (offset 2 of the Uchastkovy ore zone) are characterized by a relatively uniform distribution of gold despite a wide scatter of Au content (from 0.5 to 500 g/t). In the mineralized Uchastkovy shear zone, high-grade ore shoots are noted (Mezhov, 2000).

Within the cutoff contour of 0.4 g/t Au, all ore zones make up a single lode dipping in the northeastern direction and localized between the Main and Northwestern faults (Grigorov, 2006). At deep levels, the ore-controlling faults flatten and the ore lode becomes correspondingly flatter (Golubev, 2008).

More than 70 minerals were identified in ore of the Natalka deposit (Table 1). Quartz is the major gangue mineral. The content of ore minerals does not exceed 1–3 vol % (occasionally, 5 vol %). The ore is 95–99% composed of arsenopyrite and pyrite. The wedge-shaped and acicular arsenopyrite crystals and cubic pyrite crystals are less than 1 mm in size, sporadically being enlarged to 10–15 mm. The share of arsenopyrite decreases with depth at the expense of pyrite. The S/As ratio doubles within a 200-m vertical interval.

Au is ubiquitously detected in arsenopyrite and pyrite in amounts reaching hundreds of grams per ton. The native gold grains in quartz veins and veinlets are rather coarse. These are cloddy, stringy, tabular, spongy, and dendritic grains and crystals up to 2–3 mm or larger in size (Goncharov et al., 2002). Native gold is closely associated with arsenopyrite, galena, chalcopyrite, and sphalerite (Fig. 3). The fineness of native gold varies from 495 to 890.

Metamorphic and postmagmatic stages are recognized in the formation history of the deposit (Sidorov et al., 1994; Goryachev et al., 2000; Goncharov et al., 2002). The preore quartz and feldspar–quartz mineral assemblages are considered to be products of metamorphism of sedimentary rocks (Goncharov et al., 2002). These are low-angle veins of small thickness, which occasionally screen ore zones (Golub and Goryachev, 2005). The postmagmatic stage is subdivided into quartz–sulfide (ore) and quartz–carbonate (postore) substages. The main quartz–scheelite–pyrite–arsenopyrite assemblage, which fills veins and composes wall-rock metasomatic zones, and the sulfide–sulfosalt and quartz–stibnite assemblages were formed during the ore substage.

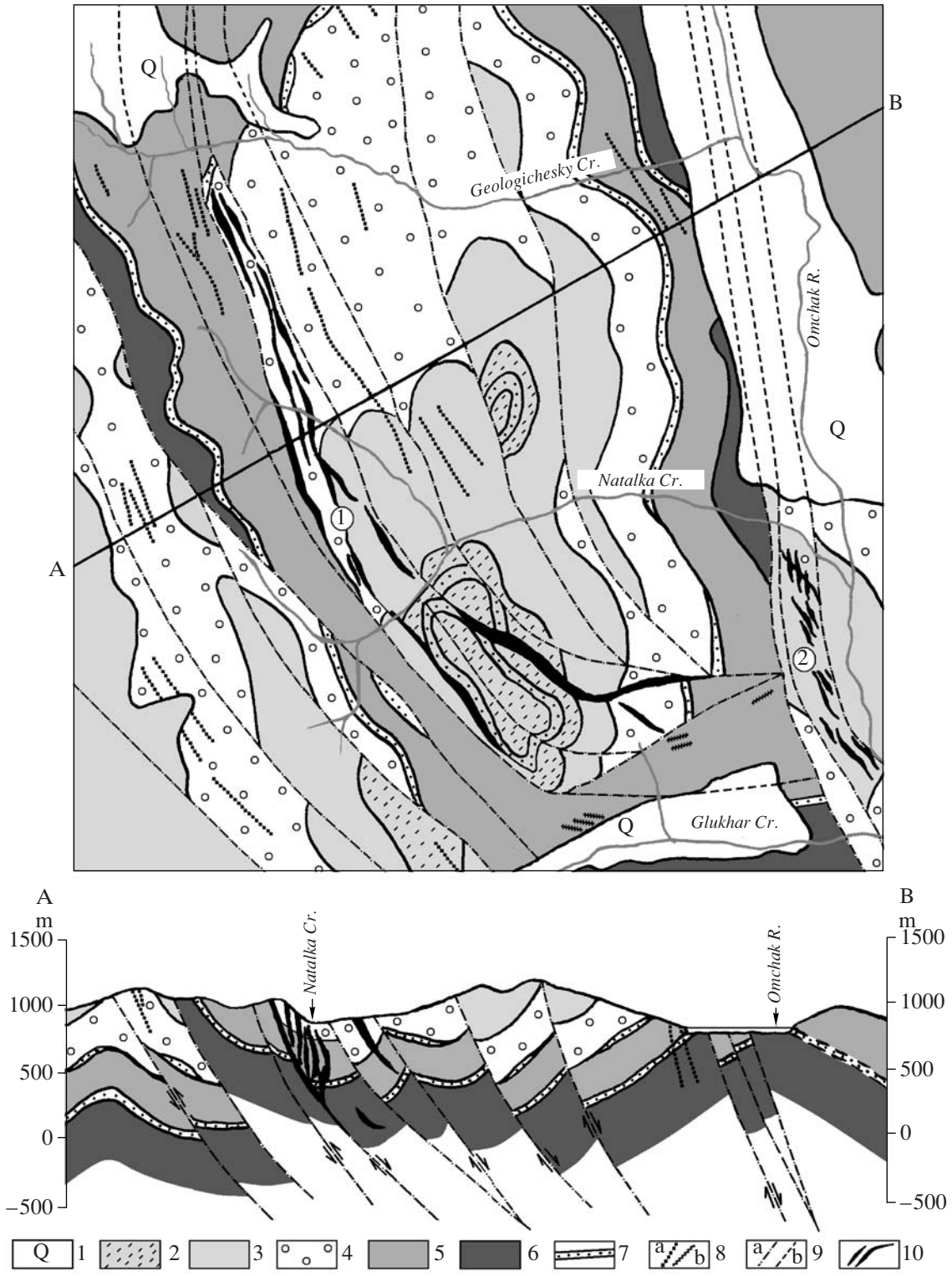

Fig. 2. Geological sketch map and geological section of the Natalka goldfield, modified after Mezhov (2000). (1) Quaternary sediments; (2–6) Permian sedimentary and volcanosedimentary rocks: (2, 3) Upper Permian Omchak Formation: (2) upper subformation: sandy siltstone, fine-grained sandstone, and silty shale, (3) lower subformation: siltstone, silty shale, and gravelstone; (4) Upper Permian Atkan Formation: siltstone with pebbles and gravel, shale, carbonaceous shale, and sandstone; (5, 6) Permian Pioner Formation: (5) upper subformation: siltstone, silty shale, fine-grained sandstone, and gravelstone, (6) middle subformation: carbonaceous and silty shales, sandstone; (7) sandstone key unit; (8) dikes: spessartite, diorite porphyry, granite porphyry, and quartz porphyry: (a) Late Jurassic and (b) Late Cretaceous; (9) faults: (a) proved and (b) inferred; (10) ore zones.

Table 1. Mineralogy of orebodies at the Natalka deposit, after Voroshin et al. (2000), Goncharov et al. (2002), and Mezhov (2000)

Type of minerals	Major minerals	Auxiliary minerals	Rare minerals	Very rare minerals
Gangue minerals	Quartz, 60–80 vol %; calcite	Dolomite, magnesite, ankerite, aragonite, anorthoclase, albite, adularia, biotite	Chlorite, sericite, kaolinite, montmorillonite, barite, apatite, scapolite, muscovite, breunnerite, siderite, titanite, epidote	Monazite, zircon
Ore minerals, 1–3, occasionally up to 5 vol %	Arsenopyrite, pyrite	Pyrrhotite, marcasite, galena, sphalerite, scheelite, chalcopyrite, native gold, ilmenite, rutile	Millerite, tetrahedrite, bournonite, boulangerite, stibnite, cobaltine, glaucodot	Acanthite, native silver, cassiterite, argentopentlandite, breithauptite, rammelsbergite

The quartz–scheelite–pyrite–arsenopyrite assemblage consists of arsenopyrite 1, pyrite, scheelite, pyrrhotite (mainly at deep levels), Ni and Co sulfoarsenides (sporadic inclusions in pyrite and arsenopyrite within ore shoots) (Golub and Goryachev, 2006), and native gold.

The sulfide–sulfosalt assemblage contains fine crystalline arsenopyrite 2, sphalerite, chalcopyrite, tetrahedrite, bournonite, boulangerite, and native gold.

The quartz–stibnite assemblage is composed of stibnite, quartz, sporadic pyrite and arsenopyrite, and

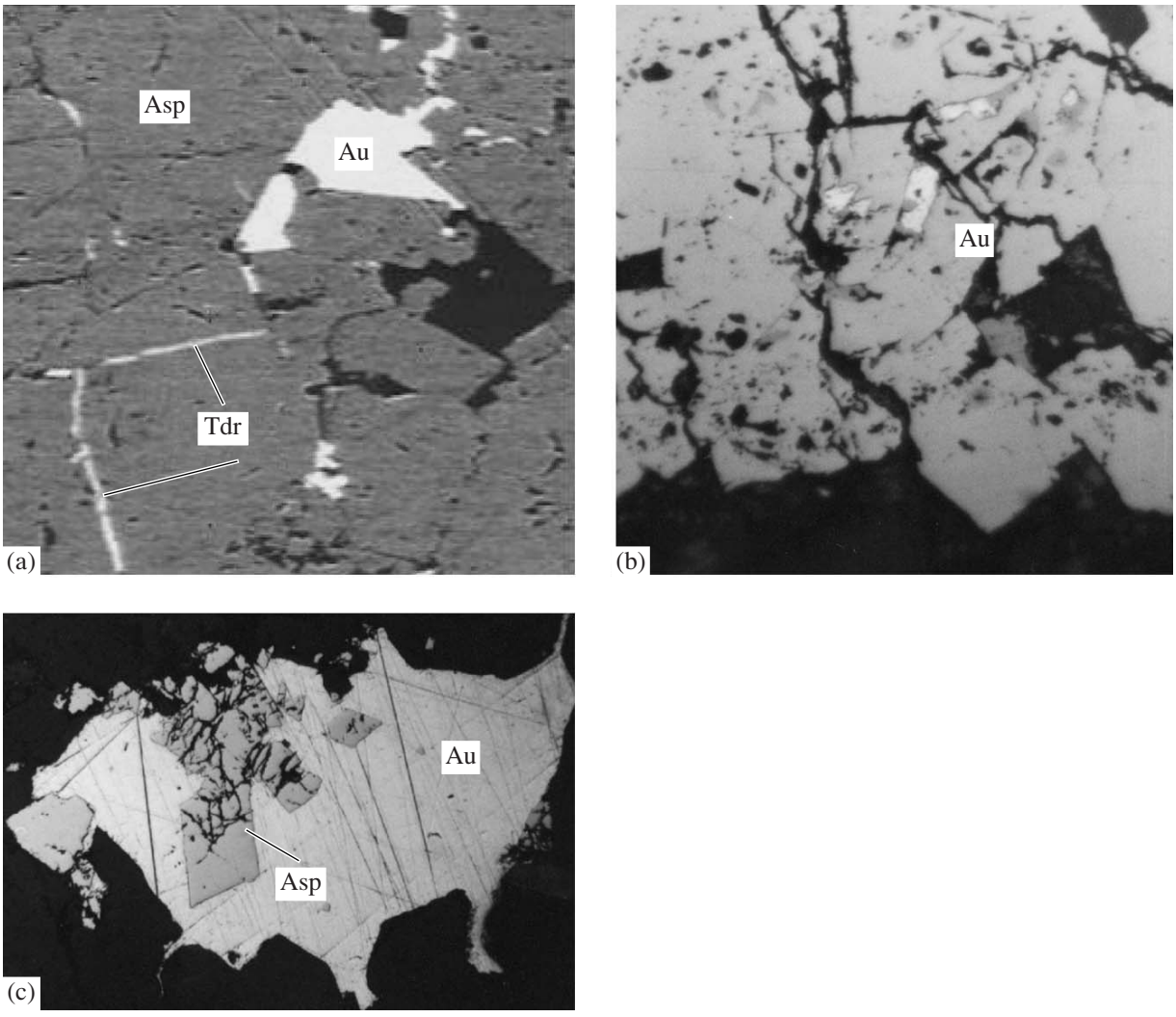

Fig. 3. Relationships between ore minerals pertaining to different assemblages: (a) arsenopyrite 1 with tetrahedrite and native gold 3 in veinlet, ore zone 64, sample 39GL-03, magn. 400; (b) native gold of low fineness in arsenopyrite 1, sample 10/99, magn. 210; (c) native gold of high fineness and arsenopyrite 2 in quartz, sample 10/99, magn. 210.

native gold and occurs at the flank of the deposit beyond the contour of economic ore.

The postore *quartz–carbonate stage* is characterized by veinlets and strings of small drusy quartz (rock crystals) and calcite, which crosscut orebodies. Kaolinite and pyrite are contained in postore veins and veinlets.

The vein quartz of the ore substage cocrystallized with arsenopyrite 1, pyrite, and scheelite. The subsequent sulfides and sulfosalts filled the interstices between quartz grains and developed along microfractures that cross these grains. At deep levels, a holocrystalline granular quartz aggregate contains small vugs lined with druses of small crystals (Goryachev et al., 2000).

HYDROTHERMALLY ALTERED ROCKS

The metasomatic alteration of rocks and formation of related ore disseminations occurred at preore and ore stages.

Carbonate metasomatism developed at the preore stage. An aureole of *carbonation* is controlled by a zone of elevated permeability that coincides with the dike field. Chlorite and then quartz are replaced with calcite, dolomite, and/or ankerite. The carbonation of host rocks unaffected by deformation is nonuniform. Sandstone interlayers underwent intense carbonation (40–45 wt % carbonates in total). Calculation of the normative mineral composition of intensely carbonated sandstone has shown that quartz is replaced most readily, with retention of the feldspar-to-sericite ratio. Microlenses and microfractures filled with pyrite and less abundant pyrrhotite were found in metasomatically carbonated rocks. They are oriented along cleavage planes and probably were formed owing to the recrystallization of diagenetic sulfides during metamorphism accompanying folding.

At the next ore stage, extended and thick zones of synore beresites with sulfide disseminations and wall-rock alteration near quartz veins developed.

Synore beresitization was established only in the Uchastkovy zone, where the alteration affected foliated terrigenous rocks that host spessartite dikes and the tectonic sutures that are natural boundaries of the ore zone. Uniformly disseminated perfectly faceted pyrite metacrystals transitional in habit from cubic to pentagonal dodecahedral are one of the main visual signs of synore metasomatic rocks. At the immediate contact with a dike of altered spessartite, pyrite is associated with abundant arsenopyrite disseminations as prismatic metacrystals up to 1 mm in size. Albite is replaced in synore beresites with sericite and quartz (Fig. 4). The degree of metasomatic alteration increases with the rate of ductile deformation up to the complete replacement of feldspars.

Synore beresitization affected spessartite dikes as well. In thick (more than 7–10 m) dikes, intense beresitization with complete replacement of chlorite with quartz, sericite, and carbonates is confined to contact zones of dikes, gradually waning toward the inner parts of dikes. Relict quartz–carbonate–sericite–chlorite metasomatic rocks of propylitic type are retained in axial zones of dikes. When the thickness of dikes is not so great, their entire volumes are involved in metasomatic alteration.

Wall-rock metasomatic rocks are typical of areas with vein-type ore mineralization, where the alteration is superimposed on both preore metasomatic rocks and synore beresites.

The main type of wall-rock alteration is carbonate–feldspar–arsenopyrite–quartz veinlets and arsenopyrite halos near the veins, where this mineral occurs as flattened metacrystals. The width of halos near separate veinlets reaches 2–4 cm; metacrystals are 0.5–1.0 mm (occasionally up to 3–4 mm) in size. Where the spacing between veinlets decreases, the elementary halos merge in wide zones of various extents and arsenopyrite contents. In morphology and composition, this generation of arsenopyrite is comparable with arsenopyrite in veins, differing only in the size of metacrystals.

In the segments affected by brittle failure, where wall-rock metasomatism is superimposed on preore metasomatic rocks, arsenopyritization is accompanied by newly formed metasomatic albite and potassium feldspar. Where thin veinlets are not so densely developed (up to 20–25 veinlets as thick as 0.5–1.0 cm per meter), being hosted in the least permeable siltstone, a small (up to 5–10%) amount of newly formed albite grains hundredths of a millimeter in size replaces only the matrix of rocks near the Uchastkovy ore zone. The feldspathization of wall rocks is limited here by a low porosity of massive siltstone. The amount of newly formed minerals appreciably increases (up to 20%) in siltstone near ore zone 3/62, where the main mass of feldspars was deposited as microveinlets within larger veins. The greatest amount of newly formed minerals (30–35%) and the complete replacement of sericite are observed in the most brittle diamictites that host ore zone 3 (Fig. 4). The recalculation of chemical compositions of chips or sawed fragments of rocks without vein mineralization to the normative mineral composition shows that the proportions of quartz, feldspar, and sericite change, with the trend being parallel to the path of replacement of sericite and quartz with feldspars. The variation of the chemical composition of more brittle rocks with quartz microveinlets deviates toward enrichment in quartz (Fig. 4).

In areas where the density and thickness of veinlets increase and near brecciated quartz veins, the intensity of metasomatic alteration of host rocks increases and is correlated with the degree of destruction. The trend of metasomatic alteration changes direction toward enrichment in quartz only (Fig. 4).

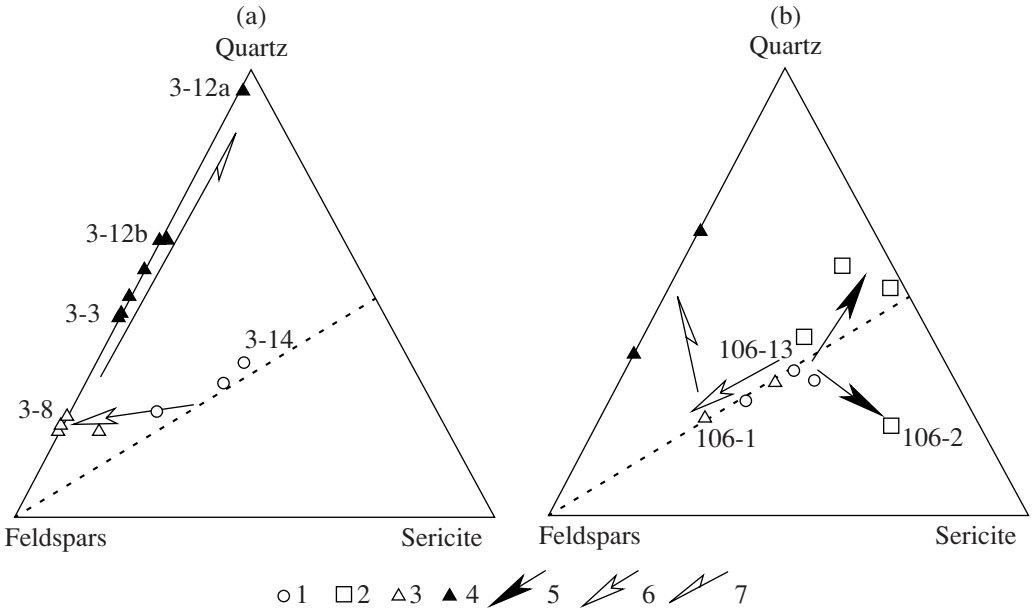

Fig. 4. Quartz, sericite, and feldspar contents (100% in total) in hydrothermally altered rocks of the Natalka deposit formed under (a) decompression and (b) compression. (1) Preore metasomatic rocks (protolith); (2) synore beresite; (3) metasomatic wall rocks with a minimal amount of vein material; (4) metasomatic wall rocks enriched in vein material; (5–7) trends of variations in mineralogy: (5) synore beresitization, (6) wall-rock metasomatism, (7) vein mineralization. 3-3, 3-8, etc., are the samples with analyzed REE.

DISTRIBUTION OF REE AND OTHER TRACE ELEMENTS IN METASOMATIC ROCKS

The REE patterns in hydrothermally altered rocks pertaining to synore beresitization, wall-rock metasomatism, and formation of veins were studied along two sections that cross ore zone 3 and the Uchastkovy zone at the level of +600 m (Fig. 5; Tables 2, 3). In addition, gabbrodiorite from the Uchastkovy zone at the south flank of the deposit (Uchastkovy Creek) and quartz porphyry along Glukhar Creek were examined.

REE were determined with ICP-MS by analysts A.V. Dubinin and S.A. Gorbacheva at the Institute of Geology of Ore Deposits, Petrography, Mineralogy, and Geochemistry, Russian Academy of Sciences (IGEM RAS) (Table 4). The detection limit was 0.0*n* ppm. The Eu (Eu/Eu*) and Ce (Ce/Ce*) anomalies were calculated from the formulas

$$Eu/Eu^* = Eu_n/(Sm_n \times (Tb_n \times Eu_n)^{1/2})^{1/2}$$

and

$$Ce/Ce^* = Ce_n/((2La_n + Sm_n)/3).$$

The tetrad effect was estimated from the formula

$$TE_{1.3} = (TE_1 \times TE_3)^{1/2},$$

where $TE_1 = (Ce_n/La_n^{2/3}Nd_n^{1/3} \times Pr_n/La_n^{1/3}Nd_n^{2/3})^{1/2}$ and $TE_3 = (Tb_n/Gd_n^{2/3}Ho_n^{1/3} \times Dy_n/Gd_n^{1/3}Ho_n^{2/3})^{1/2}$ (Irber et al., 1999).

High total REE contents (117.4–151.2 ppm) were established in *preore metasomatic rocks (protoliths)* (Fig. 6). The difference between LREE and HREE in the rocks formed under decompression ($La_n/Yb_n = 6.25$) is less than in the rocks formed under compression ($La_n/Yb_n = 12.28$). HREE in preore metasomatic rocks are fractionated only slightly ($Gd_n/Yb_n = 1.51–1.56$). The tetrad effect is the most pronounced in the third tetrad of the REE pattern ($TE_3 = 1.3$).

In *synore beresites* formed under compression, albite is replaced with sericite and quartz according to the reaction $3Ab + K^+ + 2H^+ = Ser + 6Q$ (or H_4SiO_4) + $3Na^+$. The total REE content insignificantly decreases from 151.2 to 147.9 ppm (Fig. 6a). The La_n/Yb_n ratio remains almost unchanged, being 11.44. The ore-bearing beresites are characterized by K/Rb = 295, Rb/Sr = 1.17, K/Ba = 97.2, and Ba/Rb = 3.04; K > Na.

The total REE content in *altered wall rocks*, the formation of which is accompanied by metasomatic albite and potassium feldspar, diminishes, especially in the metasomatic rocks that arose under compression, where the total REE content is almost twice as low in comparison with synore and preore beresites (Figs. 6b, 6c). The La_n/Yb_n ratio decreases by two times in the rocks formed under compression ($La_n/Yb_n = 6.17$) and slightly increases in the rocks formed under decompression ($La_n/Yb_n = 8.99$). The tetrad effect increases by up to 1.5 times. In metasomatic wall rocks, K ≪ Na. The Ba content in metasomatic wall rocks increases from 24 to 189 ppm.

The wall-rock alteration is characterized by complete replacement of sericite with feldspar and a gradually increasing share of quartz. The enrichment in SiO_2 is compensated by depletion in TiO_2, Al_2O_3, Fe_2O_3,

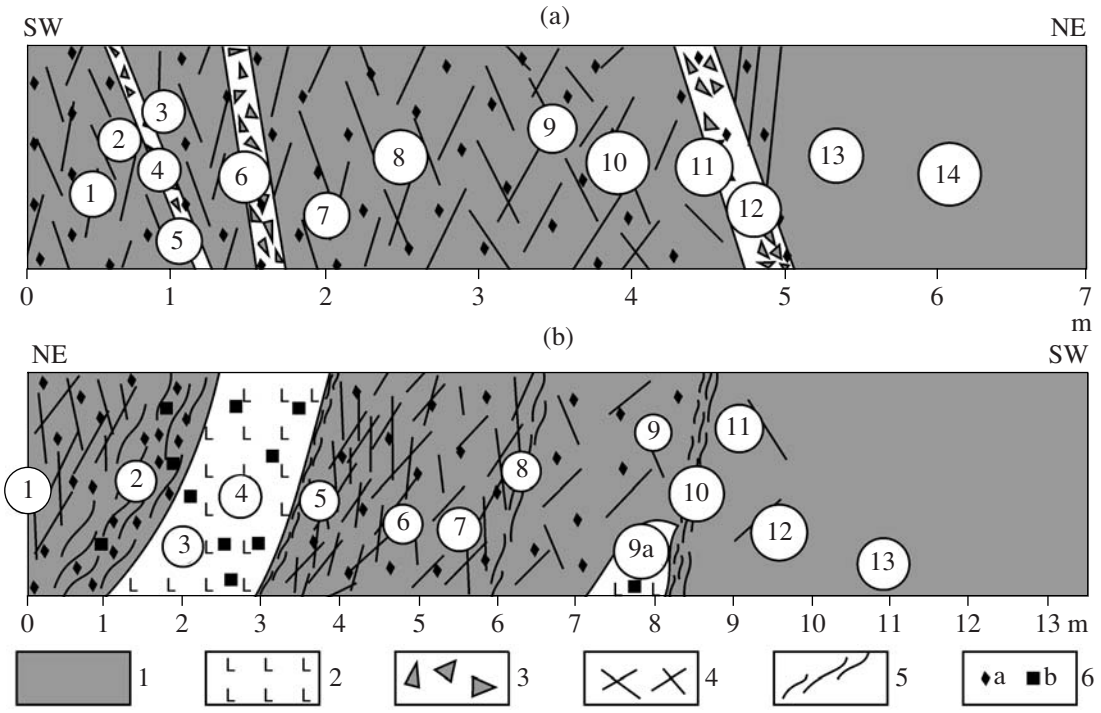

Fig. 5. The studied sections of hydrothermally altered rocks at the Natalka deposit formed under (a) decompression and (b) compression. (1) Terrigenous rocks, (2) lamprophyres, (3) brecciated quartz veins, (4) quartz veinlets with albite and arsenopyrite, (5) foliated rocks, (6) sulfidized rocks with (a) arsenopyrite and (b) pyrite. Numerals in circles are sample numbers.

MnO, MgO, Na_2O, CaO, CO_2, F, S, and As. The total REE content drops from 75.6 to 4.4 ppm, i.e., becomes two orders of magnitude lower in comparison with pre-ore beresites (Fig. 6d). With increasing degree of silicification, the La_n/Yb_n ratio first increases up to 18.55 and then gradually drops down to values established in metasomatic wall rocks in areas with a minimal number of quartz veinlets. The tetrad effect TE_3 gradually falls below the confidence level. La_n/Sm_n reaches a minimum in the intensely silicified siltstone. Eu/Eu* in vein quartz is 1.25 (sample 3-12a), indicating that crystallization proceeded from a relatively reduced mineral-forming fluid ($Eu^{3+} \ll Eu^{2+}$). The vein quartz is characterized by K/Rb = 440, Rb/Sr = 0.03, K/Ba = 9/95, and Ba/Sr = 44.2.

The REE pattern of igneous rocks occurring at the Natalka deposit is shown in Fig. 7. The total REE contents in gabbrodiorite (53 ppm) and quartz porphyry (47–67 ppm) are comparable, except for a sample of gabbrodiorite with quartz xenoliths (183 ppm) (Table 5). All rocks are enriched in LREE. The La_n/Yb_n ratio in quartz porphyry varies from 3.58 to 6.53. In gabbrodiorite, this ratio is 2.54, whereas in the gabbrodiorite sample with quartz xenoliths the ratio increases up to 16.5. No Eu or Ce anomalies are established (Eu/Eu* = 0.99–1.04; Ce/Ce* = 0.91–0.99). The REE pattern of quartz porphyry is distinguished by a moderate negative Eu anomaly (Eu/Eu* = 0.37–0.52) and by absence of appreciable Ce anomaly (Ce/Ce* = 0.88–0.97).

Thus, the REE patterns in various hydrothermal rocks at the Natalka gold deposit indicate that metasomatic rocks were formed with the participation of a relatively oxidized fluid enriched in LREE. The increasing degree of silicification is accompanied by depletion of the total REE content because feldspars and carbonates, which largely concentrate REE, are replaced with quartz. The decrease in Eu^{3+} content shows that the mineral-forming fluid is reduced owing to the interaction with host rocks, so that quartz veins are formed from a reduced fluid.

FLUID INCLUSIONS

We studied 25 vein quartz samples taken from levels 550, 600, and 650 m at the southeastern flank of the deposit from ore zones 3/62, 33, 61, 64, and the Uchastkovy ore zone with offsets. Some of these samples were collected from ore shoots. Most of the examined plates contain only very small fluid inclusions (<5 μm), which are beyond the capability of optical methods. Therefore, information is available only on eight samples (Table 6).

Characteristics of Fluid Inclusions

According to well-known criteria (Roedder, 1984), primary and secondary inclusions are distinguished. The primary inclusions are distributed uniformly in the

Table 2. Samples of hydrothermally altered rocks from the studied sections across the Natalka deposit

Interval, m	Lithology	Sample
	The Uchastkovy ore zone, crosscut 8, raise 107, gain 1, block 106, southern wall, from east to west	
0	Foliated sulfidized siltstone with thin quartz veinlets	106-1
0–2	Massive sulfidized siltstone with quartz veinlets; fine-grained pyrite combined with large (up to 2–4 mm) pyrite metacrystals	106-2
1.5	Inclined contact of sulfidized siltstone with a dike (0.5–2.0 m) intermediate in composition. The sulfide content in the dike is by an order of magnitude lower than in country siltstone	106-3
2.5	Dike with sulfide-bearing quartz–carbonate veinlets and arsenopyrite-bearing wall rock	106-4
3–4	Dike is cut by an inclined shear zone with black gouge; dike is foliated and sulfidized near the shear zone	106-5
4.5–5	Sulfidized siltstone with numerous slickensides and quartz veinlets (1–2 mm) in the shear zone	106-5a 106-6
5–6	Folded sulfidized siltstone with slickensides coated with chlorite	106-7
6–7	Similar rock enriched in quartz	106-8
8	Folded sulfidized siltstone	106-9
	A block of an altered dike affected by boudinage	106-9a
	The western contact of the Uchastkovy zone	106-10
9	Siltstone with slickensides coated with chlorite and almost devoid of sulfides	106-11
9.5	Massive siltstone with sporadic veinlets	106-12
11	Similar rock	106-13
	Ore zone 3, crosscut 19, gain 1, northern wall, from west to east	
0.5	Sulfidized diamictite with quartz–arsenopyrite veinlets	3-1
0.1–1	Brecciated inclined quartz veinlet	3-4
0.8	Sulfidized diamictite with quartz–arsenopyrite veinlets at footwall contact	3-2
1	More frequent veinlets and more intense sulfidation at the hanging wall contact	3-3
1	Quartz vein	3-5
1.5	Sulfidized and crushed diamictite at the western contact of the quartz vein (zone of merging quartz veinlets)	3-6
2	Similar rock	3-7
2.5	Diamictite with numerous quartz–arsenopyrite veinlets but depleted in arsenopyrite disseminations	3-8
3.5	Low-angle zone of metasomatic gray quartz with arsenopyrite	3-9
4	Zone of relatively rare and thin veinlets (one or two veinlets per centimeter)	3-10
4.5	Silicified and sulfidized diamictite at the footwall of a complexly built quartz–arsenopyrite vein dipping eastward	3-11
4.5–5	Substantially quartz portion of the vein in the footwall selvage along a slickenside; transition of brecciated to gray metasomatic quartz	3-12a
4.5–5	Zone of net veinlets bounded by a tectonic contact	3-12b
5	Compact diamictite almost devoid of veinlets and slightly sulfidized at the hanging contact of the vein	3-13
6	Similar rock	3-14

host mineral, whereas the secondary inclusions are related to curvilinear crosscutting fractures in quartz grains. In phase composition at room temperature, the primary inclusions are subdivided into two types (Fig. 8).

Carbon dioxide–aqueous inclusions of type I are two-phase, with liquid water and mainly liquid CO_2 at room temperature, and three-phase, containing liquid water and liquid and gaseous CO_2.

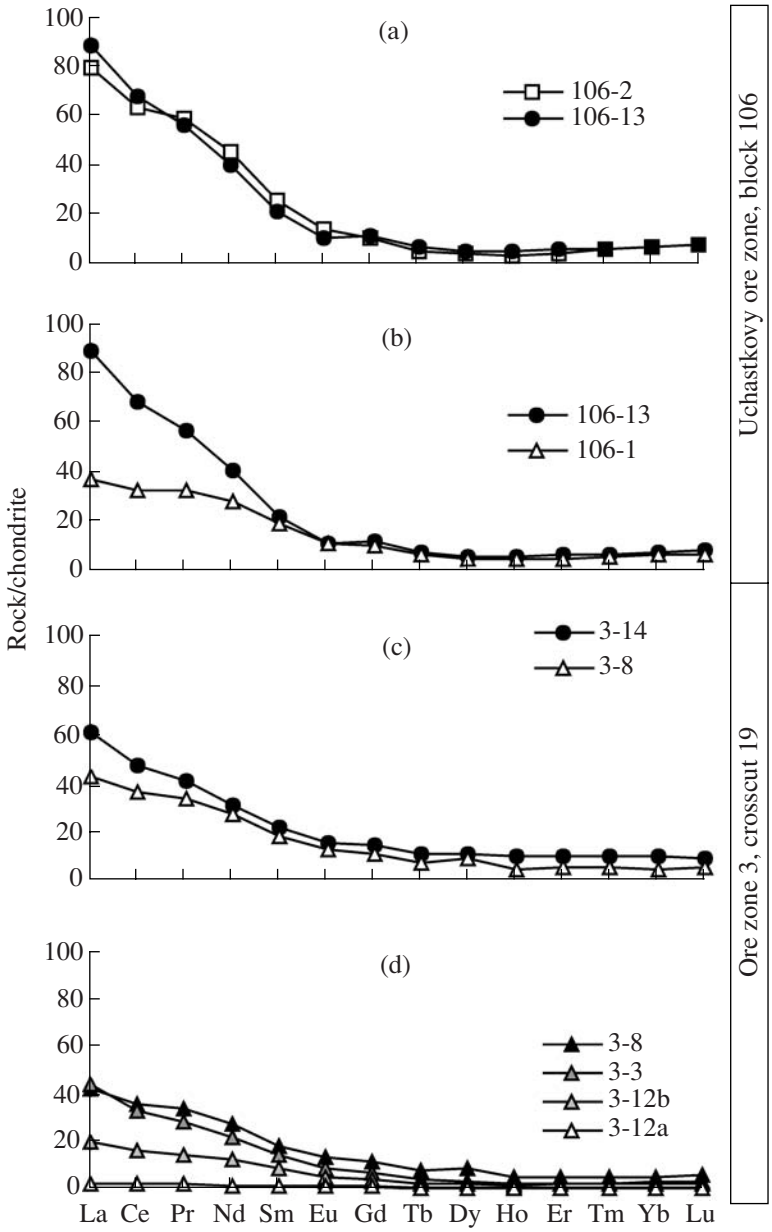

Fig. 6. Chondrite-normalized REE patterns of hydrothermally altered host rocks at the Natalka deposit: (a) synore beresitization, (b, c) wall-rock metasomatism, (d) vein mineralization. 106-2, 106-13, etc., are sample numbers.

Single-phase fluid inclusions of type II are filled with dense carbon dioxide, liquid at room temperature.

Both types of primary fluid inclusions are confined to the same growth zones of quartz and thus were captured simultaneously, when two immiscible fluids arose in the system as a result of phase separation of aqueous–carbon dioxide–salt fluid.

Rare secondary two-phase gas–liquid inclusions are classified as type III.

Research Methods

The microthermometric study of individual inclusions was carried out at IGEM RAS on a measuring complex that combines a Linkam THMSG-600 microscope heating stage (United Kingdom) with an Olympus 80$^{\times}$ long-focus objective (Japan), an Amplival microscope (Germany), a video camera, and a controlling computer.

The chemical composition of fluid entrapped into inclusions was estimated from measurements of phase transitions and transformations during heating and freezing of preparations. The accuracy of temperature measurements is ±0.2°C within an interval from –20 to +20°C and decreases with the remoteness from room temperature. The salt composition dominant in aqueous solutions was estimated from the measured eutectic temperature (T_{eut}) (Borisenko, 1977). The total concen-

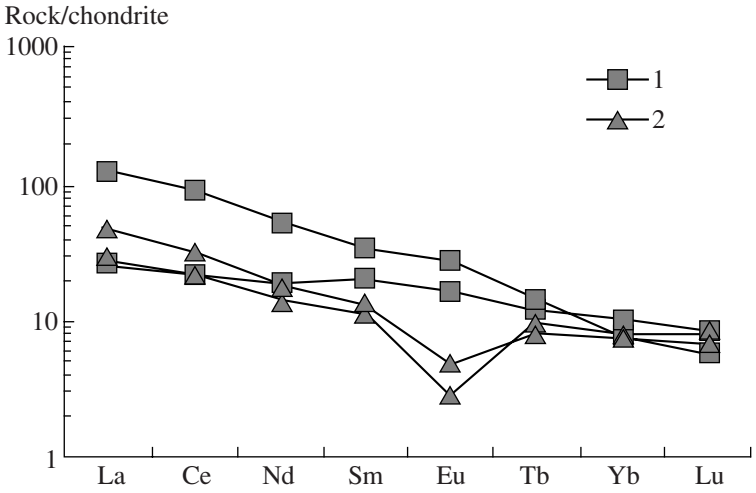

Fig. 7. Chondrite-normalized REE patterns of igneous rocks at the Natalka deposit. (1) Gabbrodiorite, (2) quartz porphyry.

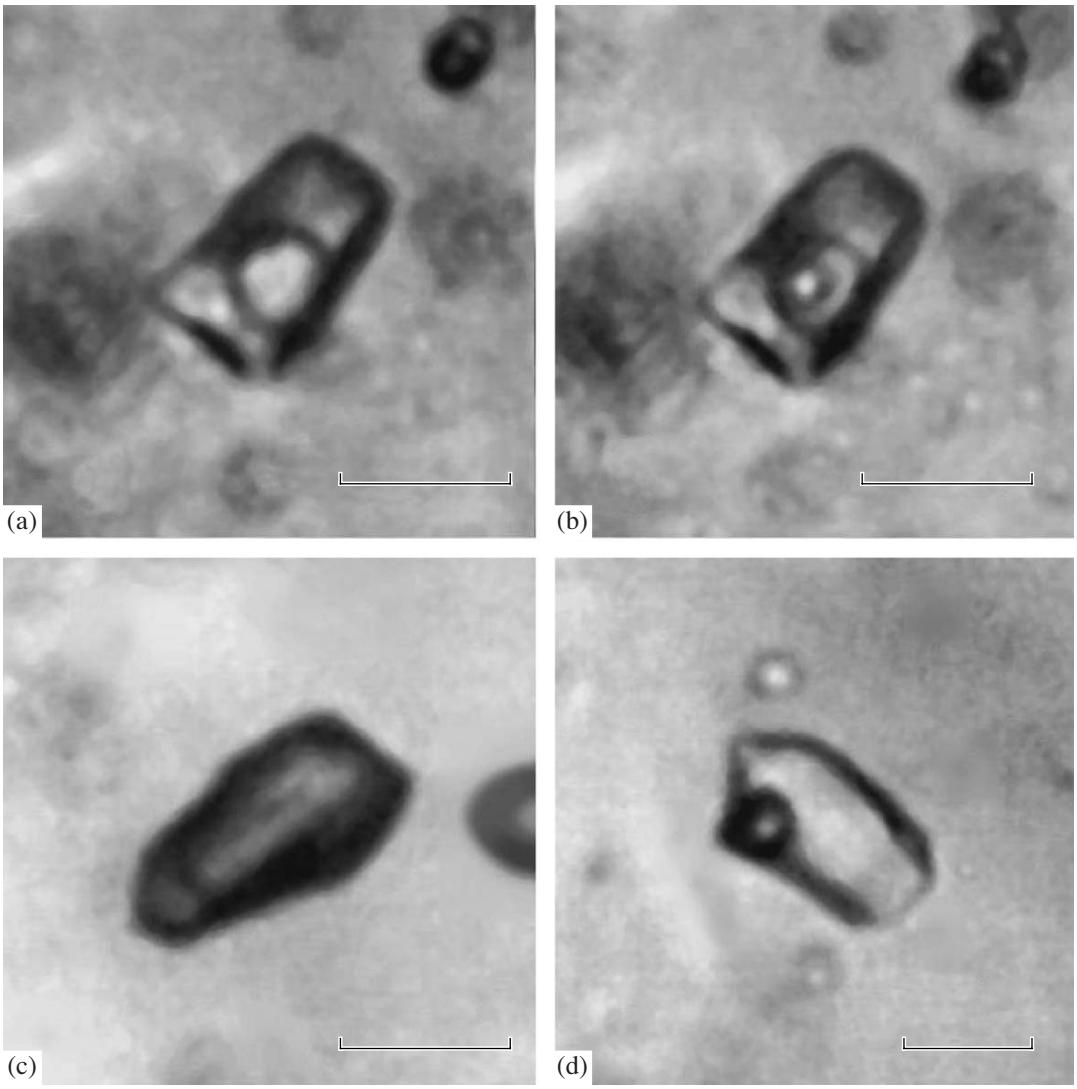

Fig. 8. Types of fluid inclusions in quartz from the Natalka deposit: (a, b) Carbon dioxide–aqueous inclusions (type I) at (a) +24 and (b) +15°C; (c) substantially gas inclusion (type II) at 24°C; (d) gas–liquid inclusion (type III) at 24°C. Scale bar, 10 μm.

Table 3. Chemical composition of hydrothermally altered rocks at the Natalka deposit, wt %

Sample	SiO_2	TiO_2	Al_2O_3	Fe_2O_3	FeO	MnO	MgO	CaO	Na_2O	K_2O	H_2O	P_2O_5	CO_2	F	S	As	Total
Uchastkovy ore zone																	
106-1	63.28	0.73	15.58	2.15	1.70	0.04	1.29	1.34	5.51	2.39	1.38	0.13	2.42	0.09	0.63	0.72	99.38
106-2	57.35	1.05	18.46	3.73	0.86	0.04	1.23	1.43	3.13	4.98	2.17	0.13	1.18	0.34	1.85	1.28	99.21
106-3	41.59	0.89	11.57	1.26	5.45	0.15	7.58	8.39	0.80	3.49	3.10	0.12	14.53	0.21	0.08	0.04	99.25
106-4	44.36	0.85	11.97	1.69	4.86	0.11	7.15	6.97	0.83	3.34	3.54	0.13	13.18	0.24	0.32	0.48	100.02
106-5	60.83	0.14	6.70	1.99	1.84	0.15	2.89	8.96	2.87	0.06	1.10	0.13	10.25	0.09	0.82	1.35	100.17
106-6	60.48	0.70	14.25	2.96	2.30	0.08	2.37	2.35	3.68	2.73	2.52	0.13	4.47	0.11	0.49	0.54	100.16
106-7	67.42	0.49	10.59	3.68	0.71	0.08	1.44	1.52	5.43	1.23	0.76	0.13	2.69	0.05	1.22	2.11	99.55
106-8	59.95	0.78	12.43	4.68	2.12	0.05	3.60	2.79	0.91	2.44	2.04	0.13	4.08	0.09	1.93	1.19	99.21
106-9	61.34	0.56	13.89	2.93	1.44	0.05	2.61	2.54	2.59	2.61	3.43	0.13	3.67	0.17	0.75	1.27	99.98
106-9a	51.80	1.00	15.07	2.90	3.17	0.06	5.14	4.60	1.17	3.56	4.57	0.13	6.58	0.27	0.15	0.15	100.32
106-10	52.77	0.58	13.58	5.01	2.88	0.06	4.88	3.81	0.24	3.07	4.98	0.13	5.88	0.18	0.81	0.87	99.73
106-11	62.00	0.69	15.51	2.82	0.70	0.04	2.42	2.41	2.83	3.76	2.89	0.14	3.38	0.15	0.00	0.02	99.76
106-12	59.57	0.64	14.43	3.93	1.00	0.02	2.95	1.83	3.20	4.25	2.26	0.10	5.27	0.12	0.02	0.00	99.59
106-13	62.67	0.60	14.43	3.47	1.13	0.04	2.61	1.92	2.78	3.75	2.00	0.12	4.35	0.10	0.00	0.00	99.97
Ore zone 3																	
3-1	63.64	0.72	13.08	3.88	0.98	0.06	1.78	1.37	5.48	3.80	0.75	0.13	2.69	0.17	0.53	0.75	99.81
3-2	79.08	0.26	6.95	2.13	0.56	0.04	0.92	1.25	3.54	0.54	0.34	0.13	1.87	0.04	0.70	1.18	99.53
3-3	71.33	0.44	8.86	3.02	0.42	0.08	1.42	1.92	5.24	0.26	0.67	0.13	3.22	0.02	0.94	1.65	99.62
3-5	75.01	0.27	7.53	2.72	0.57	0.06	1.15	1.67	4.41	0.13	0.38	0.13	2.68	0.02	0.85	1.49	99.07
3-6	73.82	0.34	8.49	2.97	0.57	0.06	1.24	1.49	5.02	0.23	0.44	0.13	2.41	0.01	0.94	1.68	99.84
3-7	73.02	0.39	9.06	1.80	1.00	0.08	1.20	1.61	5.06	0.82	1.03	0.13	2.96	0.02	0.62	0.91	99.71
3-8	63.20	0.69	12.61	3.32	1.70	0.06	1.61	1.31	5.07	3.93	0.73	0.13	2.96	0.15	0.83	1.51	99.81
3-9	63.54	0.63	11.73	2.84	1.29	0.08	1.64	2.28	5.27	3.47	0.04	0.13	4.05	0.05	0.89	1.62	99.55
3-10	62.79	0.85	14.40	1.90	3.39	0.08	1.95	1.49	5.18	3.86	1.07	0.13	2.27	0.12	0.09	0.08	99.65
3-11	62.07	0.75	13.91	2.78	2.41	0.04	2.44	2.23	3.38	2.53	2.42	0.13	3.26	0.10	0.51	0.69	99.65
3-12a	95.44	0.00	1.14	0.05	0.86	0.01	0.13	0.12	0.45	0.07	0.31	0.13	0.08	0.00	0.19	0.27	99.25
3-12b	78.88	0.24	6.88	1.50	1.12	0.06	0.89	1.28	3.58	0.58	0.30	0.13	2.14	0.02	0.72	1.28	99.60
3-13	63.40	0.96	14.81	3.67	1.55	0.10	2.22	1.37	4.71	3.40	1.30	0.13	1.89	0.07	0.05	0.01	99.64
3-14	64.12	0.97	14.99	3.52	1.57	0.10	1.61	1.90	3.98	2.98	2.15	0.13	1.37	0.07	0.05	0.00	99.51

Note: Analyses were performed at the chemical analysis laboratory of the Institute of Geology of Diamond and Noble Metal Deposits, Siberian Branch, Russian Academy of Sciences.

Table 4. REE contents, ppm, in metasomatic rocks of the Natalka deposit

Element	1	2	3	4	5	6	7	8
	106-1	106-2	106-13	3-3	3-8	3-12a	3-12b	3-14
La	13.6	29.3	32.7	16.2	15.7	0.8	7.2	22.3
Ce	30.8	61.5	65.9	31.2	34.7	1.7	15.2	45
Pr	4.44	8.13	7.72	3.86	4.64	0.24	2	5.66
Nd	19.7	32.8	28.7	15.7	19.6	0.9	8.5	22.2
Sm	4.35	5.95	4.95	3.18	4.24	0.22	1.92	5
Eu	0.92	1.25	0.93	0.77	1.11	0.05	0.41	1.33
Gd	3.01	3.32	3.46	2.08	3.36	0.17	1.25	4.49
Tb	0.34	0.3	0.4	0.21	0.42	0.005	0.13	0.65
Dy	1.74	1.64	2.19	0.91	3.31	0.12	0.63	4.11
Ho	0.36	0.34	0.43	0.18	0.42	0.02	0.12	0.88
Er	1.1	1.12	1.5	0.52	1.27	0.06	0.37	2.6
Tm	0.2	0.22	0.22	0.08	0.18	0.01	0.06	0.37
Yb	1.49	1.73	1.8	0.59	1.18	0.06	0.42	2.41
Lu	0.25	0.3	0.32	0.11	0.2	0.01	0.07	0.36
Total	82.3	147.9	151.2	75.6	90.3	4.4	38.3	117.4
Eu_n/Eu_n^*	0.87	0.96	0.79	1	0.96	1.25	0.91	0.91
Ce_n/Ce_n^*	1.04	1.04	1.03	0.96	1.05	1	1	0.99
La_n/Yb_n	6.17	11.44	12.28	18.55	8.99	9.01	11.58	6.25
La_n/Sm_n	1.97	3.1	4.16	3.21	2.33	2.29	2.36	2.81
Gd_n/Yb_n	1.64	1.56	1.56	2.86	2.31	2.3	2.41	1.51

Note: Metasomatic rocks formed under decompression (1–3) and compression (4–8); 106-1, etc., are sample numbers.

tration of salts in fluid inclusions of type III was estimated from the temperature of ice melting on the basis of experimental data for the NaCl–H_2O system (Bodnar and Vityk, 1994). The salt concentration in inclusions with a high CO_2 content (type I) was estimated from the melting temperature of gas hydrates (Collins, 1979; Darling, 1991) because most values of the gas hydrate melting temperature were below +10°C. The pressure was determined for heterogeneous fluids by the intersection of the isochore and isotherm (Kalyuzhny, 1982). The salt concentration, density, and fluid pressure were estimated using the FLINCOR program (Brown, 1989).

In the cases where fluid inclusions are captured under conditions of phase separation, i.e., on the line of two-phase equilibrium, the estimation of the true temperature does not require correction of measured temperatures for pressure (Roedder, 1984). Therefore, the homogenization temperatures of primary inclusions were considered as the temperatures of quartz crystallization.

Results of Microthermometric Study

As follows from the examination of 167 individual fluid inclusions (Table 6; Fig. 9), the homogenization temperatures of inclusions pertaining to type I vary from 363 to 280°C. The salt concentration in these inclusions was estimated as 1.0–4.9 wt % NaCl equiv from the melting temperature of CO_2 gas hydrate. The CO_2 concentration in ore-forming fluid was rather high and ranged from 8.8 to 2.1 mol/kg of solution (fluid density 1.02–0.87 g/cm^3). Judging from the eutectic temperature of –38 to –21°C, Na and Mg chlorides were dominant in the ore-forming fluid. A weak tendency toward an increase in the salt concentration with decreasing temperature should be noted.

In inclusions of type II, carbon dioxide is homogenized into the liquid phase at a temperature of –5.3 to +27.7°C. Carbon dioxide melts in the temperature range from –57.9 to –59.9°C, which is lower than the melting temperature of pure CO_2 (–56.6°C). The density of the gas phase is rather high and varies from 0.67 to 0.92 g/cm^3.

The fluid pressure estimated for fluid inclusions pertaining to types I and II varies from 2430 to 1120 bar at temperatures ranging from 363 to 287°C (Table 6).

The fluid inclusions of type III were homogenized into liquid at 205–283°C (Fig. 9). The eutectic temperature varies from –25 to –34°C, testifying to the pre-

Table 5. Chemical composition of igneous rocks at the Natalka deposit

Component	1	2	3	4
	1502-B-01	1503-B-01	1504-B-01	1419-B-00
Na_2O, wt %	1.62	2.5	0.16	3.33
MgO	10.31	9.58	0.23	0.23
Al_2O_3	12.51	10.97	17.71	14.25
SiO_2	43.88	46.35	78.66	75.72
K_2O	1.02	0.95	3.3	3.3
CaO	9.5	7.4	0.19	0.72
TiO_2	1.49	1.92	0.04	0.05
MnO	0.135	0.144	0.024	0.034
Fe_2O_3	10.83	10.11	1.14	1.4
P_2O_5	0.105	0.823	0.037	0.045
S	0.15	0.31	0.18	0.02
Total	91.55	91.06	101.67	99.1
Cr, ppm	703	342	10	61
Sc	43	27	2	0
V	342	209	8	2
Co	36	33	6	7
Ni	192	236	7	4
Rb	33	40	109	82
Sr	305	979	21	113
Y	24	21	25	16
Zr	71	223	44	56
Nb	2	37	14	9
Ba	334	7129	638	938
La	9.6	44.8	10.2	17.4
Ce	20.8	87.6	20.7	30.5
Nd	13.2	37.3	10.3	13.1
Sm	4.58	7.97	2.6	3.11
Eu	1.44	2.33	0.25	0.41
Tb	0.7	0.79	0.55	0.47
Yb	2.5	1.8	1.9	1.8
Lu	0.31	0.21	0.3	0.25
REE in total	53.15	182.85	46.88	66.96
Eu/Eu*	0.99	1.04	0.37	0.52
Ce/Ce*	0.91	0.99	0.97	0.88
La_n/Yb_n	2.54	16.5	3.58	6.53
La_n/Sm_n	1.31	3.54	2.48	3.52
K/Rb	251	334	248	198
K/Ba	43	29	27	1
Ba/Rb	5.85	11.44	9.19	178.23
Rb/Sr	0.19	0.73	0.22	0.04

Note: (1) gabbrodiorite; (2) gabbrodiorite with quartz xenoliths; (3, 4) quartz porphry; 1502-B-01, etc., are sample numbers.

dominance of Na and Mg chlorides in the aqueous salt solution. The salt concentration estimated from the melting temperature of ice is 5.4–7.0 wt % NaCl equiv. The density of such fluids was 0.80–0.91 g/cm^3. Because secondary fluid inclusions and sulfide–sulfosalt aggregates are related to the same tortuous fractures in quartz, it cannot be ruled out that minerals of the sulfide–sulfosalt assemblage precipitated from fluid entrapped in these inclusions.

The previously published results of fluid inclusion studies in quartz from the Natalka deposit show a wider range of homogenization temperatures (410–80°C); fluid inclusions were classified as carbon dioxide–aqueous and substantially carbon dioxide; the pressure was estimated at 1100–450 bar (Goncharov et al., 2002). The examination of aqueous extracts showed a low concentration of salts (30–21 g/l). CO_2, CO, H_2, N_2, CH_4, and other compounds were detected with gas chromatography of bulk samples. Bicarbonate–water, substantially gaseous carbon dioxide, and aqueous salt solutions were identified as fluid inclusions (Struzhkov et al., 2006). The fluid inclusions captured by the early, preore quartz were homogenized at 385–300°C. The fluid pressure was estimated at 500–800 bar. The Au-bearing mineral assemblages precipitated at 250–300°C and 300–500 bar from bicarbonate aqueous fluid with a salinity of 4–9 wt % NaCl equiv. The homogenization temperature of salt-bearing aqueous fluid inclusions varied from 130 to 225°C and their salinity was estimated at 5–8 wt % NaCl equiv. The authors of the publications cited above did not report the equipment used and the methods of salinity and pressure calculation; therefore, the reasons for discrepancies in the estimated parameters, particularly, in fluid pressure, remain unclear. It cannot be ruled out that obsolete density properties of carbon dioxide were used.

Thus, despite some differences in the results, all investigations have shown that compositionally contrasting fluids with low to moderate salinity were captured as fluid inclusions in quartz.

OXYGEN ISOTOPIC COMPOSITION

Oxygen isotopic composition of quartz. The $\delta^{18}O$ values were determined for vein quartz of the quartz–scheelite–pyrite–arsenopyrite assemblage (16 determinations) and the sulfide–sulfosalt assemblage (9 determinations) of the quartz–sulfide stage from ore zones at deep levels of the southeastern flank of the Natalka deposit (Table 7). The measurements were carried out by isotopic ratio mass spectrometry (IRMS) on a DELTA^{plus} apparatus (Finnigan) at IGEM RAS (analyst A.A. Avdeenko). The NBS-28 silicate standard was used. The oxygen isotope ratio was measured in CO_2 gas released on interaction of quartz with BrF_5 at 600°C and then with a heated graphite rod. The results are presented as $\delta^{18}O$ values relative to SMOW. The measurement uncertainty was ±0.05‰.

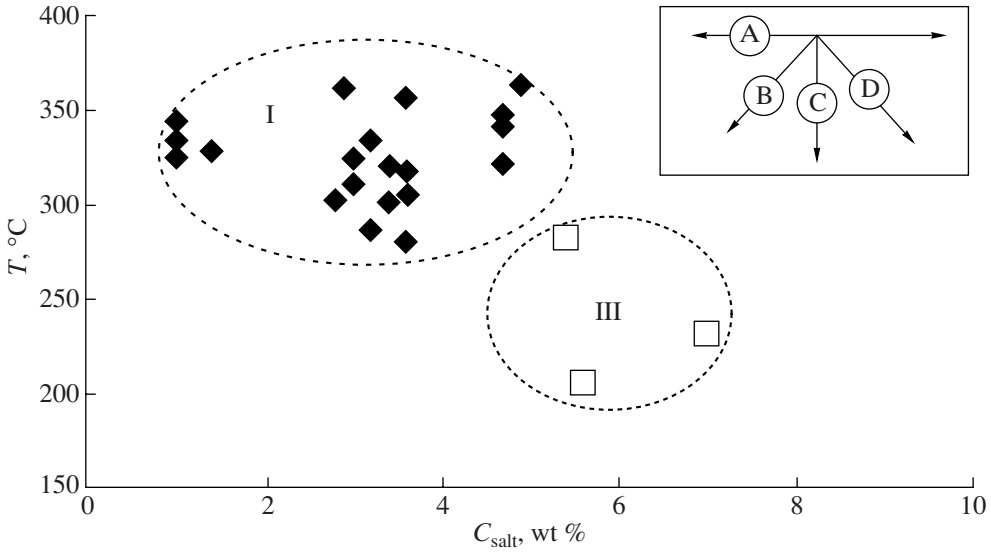

Fig. 9. Temperature versus salinity in fluid inclusions at the Natalka deposit. (I, III) Types of fluid inclusions. Typical trends in coordinates T_{hom}–salinity are shown in the inset. Letters in circles: (A) immiscible fluids, (B) mixing of fluids, (C) cooling, (D) boiling with cooling (Kreuzer, 2005).

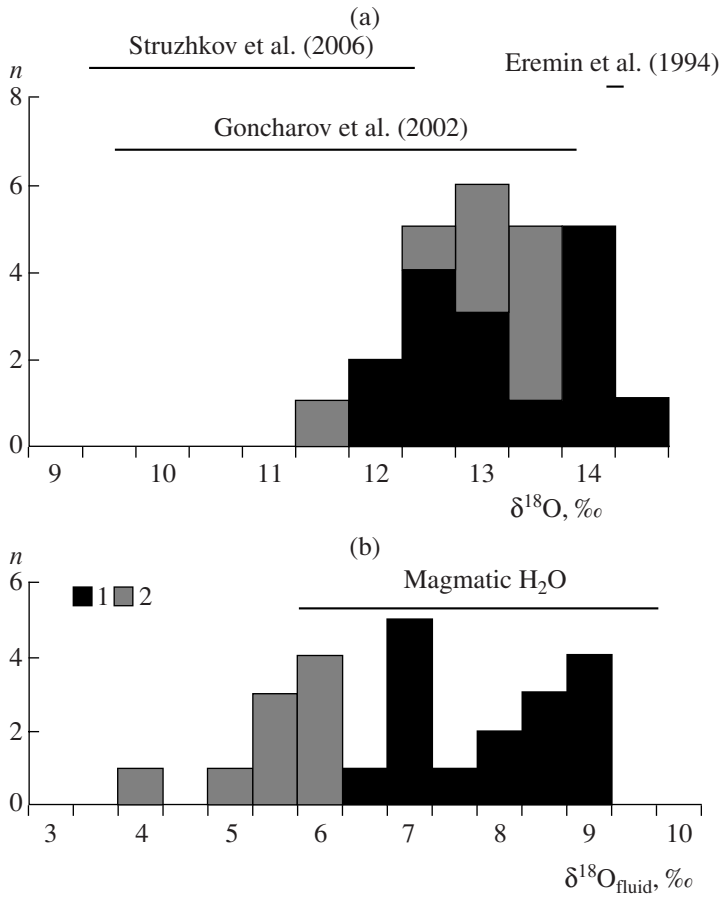

Fig. 10. Oxygen isotopic composition of quartz and ore-forming fluid at the Natalka deposit. Mineral assemblages: (1) quartz–scheelite–pyrite–arsenopyrite, (2) sulfide–sulfosalt.

Table 6. Results of heating and freezing studies of individual fluid inclusions in quartz from ore veins at the Natalka gold deposit

Sample	Mineral	Inclusion type**	*n*	T_{hom}, °C	T_{eut}, °C	$T_{ice\ melt}$, °C	$T_{CO_2\ melt}$, °C	$T_{CO_2\ hom}$, °C	$T_{gas\ hydrate}$, °C	C_{salt}, wt % NaCl equiv	C_{CO_2}, mol/kg of solution	D, g/cm^3	P, bar
25-04	Quartz	I	4	361–321	–35…–21	–1.7…–1.5	–59.2	n.d.	7.6	2.9–4.7	–	0.59–0.68	–
	″	III	9	283–233	–31…–25	–3.3…–4.4	–	–	–	5.4–7.0	–	0.80–0.89	–
29-2	Quartz*	I	18	334–280	–34…–32	–5.7…–4.4	–58.5…–59.0	25.0 L…23.8 G	8.4–8.2	3.2–3.6	6.6–2.1	0.96–0.89	1750–1250
	″	II	18	–	–	–	–58.4…–58.7	17.5…22.7 L	–	–	–	0.79–0.74	
	Quartz	III	3	205	–34	–3.4	–	–	4.1	5.6	–	0.91	–
33-04	Quartz*	I	8	301	–34	–4.9	–59.6	25.2 L	8.3	3.4	4.2	0.93	1370
	″	II	2	–	–	–	–59.7	21.6 L	–	–	–	0.76	
7-1	″	I	20	343–320	–35…–31	–4.4…–3.6	–59.9…–59.3	–5.3…24.4 L	9.5–8.3	1.0–3.4	8.4–5.9	1.02–0.88	2430–1240
	″	II	13	–	–	–	–59.6…–59.9	3.6…26.1 L	–	–	–	0.91–0.69	
16-1	Quartz*	I	7	363–356	–30…–31	–9.0…–4.1	–58.4…–58.7	17.4…11.7 L	7.5–8.2	3.6–4.9	6.8	1.01	2260–1930
	″	II	8	–	–	–	–58.8…–58.6	11.6…16.4 L	–	–	–	0.85–0.81	
7-04-2	″	I	8	324–311	–38	–4.9	–59.0	26.4 L	8.5	3.0	3.7	0.87	1600–1120
	″	II	14	–	–	–	–58.9…–59.2	19.4…27.4 L	–	–	–	0.78–0.67	
35-2	″	I	13	332–302	–35…–29	–4.9…–4.6	–59.1…–58.4	19.6 L	10.3–8.6	1.0–2.8	8.1–5.4	0.97–0.80	2430–1610
	″	II	6	–	–	–	–57.9…–59.9	1.8…16.3 L	–	–	–	0.92–0.81	
11-04	″	I	7	348–341	–34	–4.2	–58.2	24.9 L	7.6	4.7	6.4	0.93	1780–1600
	″	II	13	–	–	–	–59.5…–59.0	18.5…21.3 L	–	–	–	0.79–0.76	

Note: * heterogeneous fluid; ** inclusion types: (I) carbon dioxide–aqueous, (II) gas, (III) two-phase gas–liquid; *n*, number of inclusions, *D*, density, L, homogenization of dense carbon dioxide into liquid and G, into gas; n.d., not determined.

Table 7. The studied samples of quartz from the Natalka deposit

Sample	Ore zone (offset)	Level, m	Vein thickness, m	Quartz characteristics	Ore mineralization
1-GL-03	Uchastkovy (2)	550	5–6	Light gray, massive	Au (up to 0.8 mm), Sph, Asp, Ga
2-GL-03	Uchastkovy (2)	585	6–9	Massive	Au (up to 0.8 mm), Asp, Ga, Py (2–3 vol %)
7-GL-03	64	635	1–2	Massive, passing into drusy, locally crushed	Asp (<1 vol %)
10-GL-03	64	640	Up to 5	Light gray, massive	Py, Asp
12-GL-03	61	600	Up to 8	″	Py, Asp
14-GL-03	61	613	5–6	Light gray, up to transparent, drusy	Au (up to 1.5 mm), Sph, Asp, Ga, Chp
17-GL-03	64 (2)	617	1–1.5	Light gray, up to transparent, drusy, locally passing into massive and less frequently into confluent	Py, Asp
22-GL-03	64 (3)	615	5–6	Light gray, up to transparent, drusy	Single Asp, Ga, and Sph grains
25-GL-02		650	2–2.5	Light gray, massive	Py, Asp
29-GL-03	3-62 (1)	600	9–12	Light gray, massive, locally passing into drusy	Asp, Ga, Sph (<1 vol %)
30-GL-03	3-62 (1)	585	15–20	Light gray to gray, massive, passing into drusy	Au (up to 0.3 mm), Asp, Ga, Sph, Py (2–3 vol %)
31-GL-03	64	650	1–2	Light gray, massive, locally passing into drusy	Asp (<1 vol %)
34-GL-03	64 (3)	613	Up to 0.5	Light gray to gray and transparent, massive, passing into drusy	Single Asp, Ga, Sph
39-GL-03	64	640	1.5–2	Drusy	Py, Asp, Au (up to 1.2 mm, cloddy, extending along vein contact)
3-GR-99	Uchastkovy (2)	600	Up to 20	Zonal: milk white fine crystalline–gray, up to dark gray metasomatic (5–15 cm)–network of microveinlets Microvugs with rock crystals	Asp, Ga, Sph, Au (up to 1 mm, light yellow)
8-GR-99	64 (2)	600	Up to 5	Zone of net veinlets; confluent, white milk, drusy	Asp, Py, Sph (single grains), Au (<0.2 mm, sporadic grains in drusy quartz)
9-GR-99	3-62	600	20–30, 1–5, pseudoveinlets	From dark to light gray and milk white, confluent	Asp (up to 10 vol %), Py, scheelite (2–3 to 10 mm), Au (<0.5 mm, sporadic grains along the boundary between light gray and milk white quartz)
11-GR-99	64	650	Up to 10	White milk, granular	Rare Au and Ga disseminations (selvages), single Chp grains in central part
13-GR-99	3-62	650	Up to 10	Light gray to white, massive	Py, Asp, scorodite
NT-13-01	3-62 with offsets	575	Up to 5	Light gray, massive	Py, Asp
NT-14-01	3-62 with offsets	575	10–15	Massive, locally passing into drusy	Asp (up to 2 mm) (<1 vol %)
NT-17-01	Uchastkovy	600	1.5–2	From light to dark gray, massive	Single Asp grains
NT-22-01	64	600	Up to 0.5	Zone of veinlets, fine crystalline, locally passing into drusy	Asp

Note: (Asp) arsenopyrite, (Py) pyrite, (Sph) sphalerite, (Ga) galena, (Chp) chalcopyrite, (Au) native gold.

Table 8. Oxygen isotopic composition of quartz and equilibrium fluid at the Natalka deposit

Sample	Ore zone (offset)	Level, m	$\delta^{18}O_{quartz}$, ‰	$\delta^{18}O_{fluid}$, ‰
Quartz–pyrite–arsenopyrite assemblage				
9-GR-99	3-62	600	+13.7	+8.4
13-GR-99	3-62	650	+11.9	+6.6
NT-13-01	3-62	575	+12.0	+6.7
NT-14-01	3-62	575	+13.6	+8.3
NT-17-01	Uchastkovy	600	+12.2	+6.9
NT-21-01			+13.9	+8.6
NT-22-01	64	600	+11.6	+6.3
NT-23-01			+12.1	+6.8
7-GL-03	64	635	+14.1	+8.8
10-GL-03	64	640	+12.6	+7.3
12-GL-03	61	600	+14.0	+8.7
17-GL-03	64 (2)	617	+13.5	+8.2
22-GL-03	64 (3)	615	+14.0	+8.6
25-GL-03		650	+12.3	+7.0
31-GL-03	64	650	+12.9	+7.5
39-GL-03	64	640	+12.9	+7.6
Quartz–sulfide–sulfosalt assemblage				
3-GR-99	Uchastkovy (2)	600	+12.9	+5.3
8-GR-99	64 (2)	600	+12.7	+5.1
11-GR-99	64	650	+11.2	+3.6
1-GL-03	Uchastkovy (2)	550	+13.3	+5.7
2-GL-03	Uchastkovy (2)	585	+13.5	+5.9
14-GL-03	61	613	+13.4	+5.8
29-GL-03	3-62 (1)	600	+12.7	+5.1
30-GL-03	3-62 (1)	585	+12.2	+4.6
34-GL-03	64 (3)	613	+13.3	+5.7

The $\delta^{18}O$ values of quartz from the quartz–scheelite–pyrite–arsenopyrite and sulfide–sulfosalt assemblages are practically indiscernible and vary from +11.6 to +14.1‰ and +11.2 to +13.5‰, respectively (Fig. 10a; Table 8). The results obtained are comparable with previously published estimates: +14.0 ± 0.1‰ (Eremin et al., 1994), +9.3 to +13.6‰ (Goncharov et al., 2002), and +9.1 to +12.2‰ (Struzhkov et al., 2006). These values are similar to the oxygen isotopic composition of quartz at other gold deposits from the northeast of Russia (Goryachev, 2003), including the Nezhdaninsky and Maisky superlarge deposits (Bortnikov et al., 1998, 2004, 2007). These data also fall into the interval of $\delta^{18}O$ of quartz from Phanerozoic mesothermal gold deposits (+12 to +18‰) (Bortnikov, 2006; Kerrich, 1990; Ridley and Diamond, 2000).

The oxygen isotopic composition of fluid was calculated using the measured $\delta^{18}O$ values of quartz and the homogenization temperature of fluid inclusions in this mineral: $\delta^{18}O_{quartz} - \delta^{18}O_{H_2O} = 3.34(10^6/T^2) - 3.31$ (Matsuhisa et al., 1979). $\delta^{18}O$ of ore-forming fluid at the Natalka deposit could have ranged from +6.3 to +8.8‰ at 350°C during crystallization of the early mineral assemblage and from +3.6 to +5.9‰ at 280°C at the moment of deposition of the late mineral assemblage (Fig. 10b, Table 8). According to Voroshin et al. (2000), $\delta^{18}O_{H_2O}$ varies from +7.1 to +7.3‰ at 300°C. The calculated $\delta^{18}O_{H_2O}$ of mineral-forming fluid is consistent with the oxygen isotopic composition of quartz from other large and superlarge gold deposits of Russia (Bortnikov, 2006; Bortnikov and Prokof'ev, 2007), as well as from Precambrian and Phanerozoic orogenic gold deposits worldwide (+6 to +11‰ and +7 to +13‰, respectively) (Goldfarb et al., 2005).

DISCUSSION

The REE patterns in rocks, the results of fluid inclusion study, and the oxygen isotopic composition were used for ascertaining the composition of the mineral-forming fluid and its formation conditions and sources at the Natalka deposit.

The REE patterns are controlled by the physicochemical conditions of mineral crystallization, their crystal chemical features, and composition of mineral-forming fluid. Nevertheless, it may be suggested that REE patterns in metasomatic rocks reflect the REE distribution in hydrothermal fluid at the moment of mineral formation. The composition of the protolith, as well as the composition and pH of the solution, are crucial for the formation of metasomatic rocks; temperature, pressure, and other parameters are less important (*Metasomatism*…, 1998). It is evident that these parameters exert an effect on the behavior of REE. In general, the metasomatic alteration of rocks is accompanied by their enrichment in LREE, which is typical, for example, for potassic metasomatism (Balashov, 1976; Taylor and Fryer, 1982, Sazonov et al., 2006). The prevalence of LREE over HREE is caused by a greater migration ability of the latter. The REE solubility in fluid containing K, Na, Fe, and Al extracted from rocks increases, probably, due to the formation of complex compounds. The degree of REE concentration in the postmagmatic solution is controlled not only by the mobility of REE themselves, but also by the relative solubility of other, especially major, components in comparison with REE (Balashov, 1976).

The REE patterns of metasomatic rocks in comparison with those of the Permian siltstones in the Natalka goldfield (Tyukova et al., 2007) are shown in Fig. 11. In metasomatic rocks formed under decompression, the LREE and HREE contents gradually decrease relative to the REE contents in siltstone. The REE patterns of

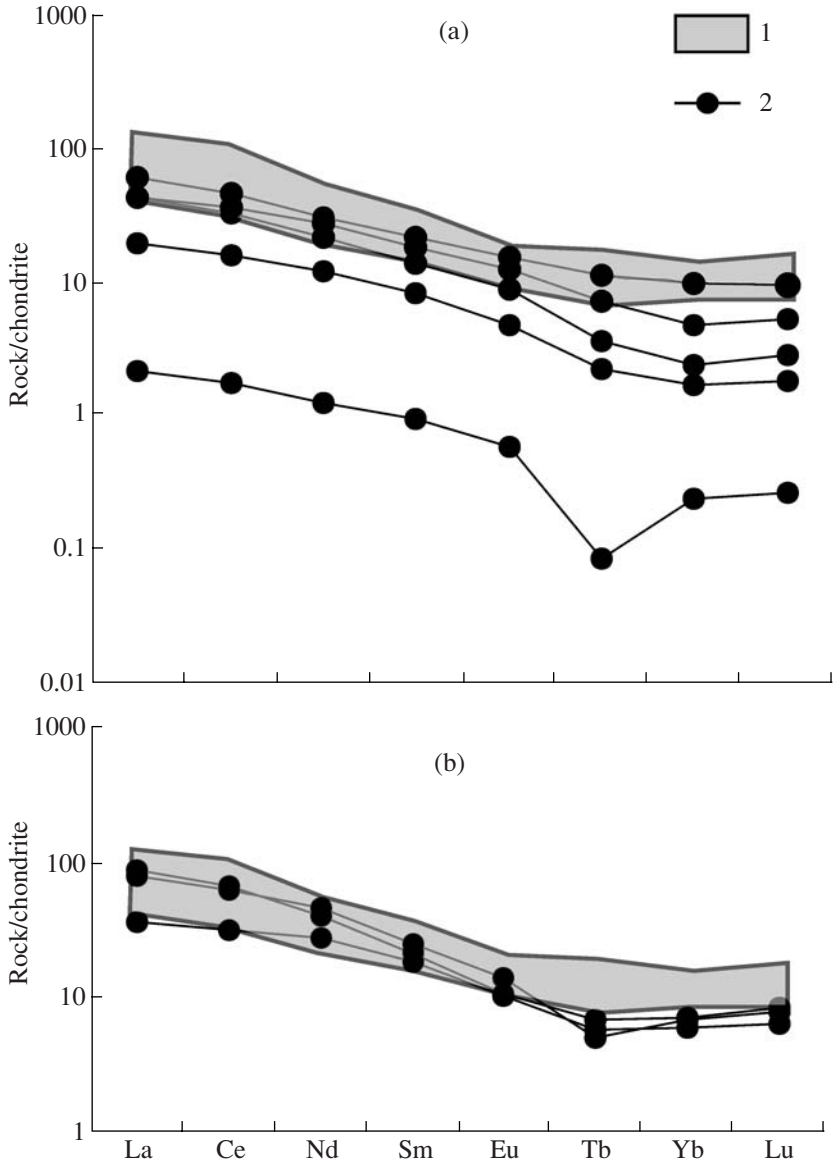

Fig. 11. Chondrite-normalized REE patterns of sedimentary and metasomatic rocks formed under (a) decompression and (b) compression at the Natalka deposit. (1) Siltstone, (2) metasomatic rocks.

metasomatic rocks formed under compression are uniform as concerns HREE and characterized by slight depletion in LREE. The metasomatic rocks are depleted in Tb, Yb, and Lu. The progressive extraction of REE with increasing intensity of rock alteration could have been caused by fluids of magmatic origin (Lottermoser, 1992) or fluids of meteoric origin (Taylor and Fryer, 1982). At the early stage, high-temperature postmagmatic fluids with a prevalence of Cl^-, high pH, and low water/rock ratio facilitate LREE dissolution. At the late stage, with decreasing temperature and pH of the solution and an increasing water/rock ratio, fluids containing CO_3^{2-}, F^-, Cl^-, and PO_4^{3-} provide an abrupt increase in mobility of all REE. At low pH, LREE and Eu^{2+} are the most soluble in chloride solutions, whereas HREE form complexes with CO_3^{2-} and F^-. The effect of meteoric water also leads to the leaching of all REE with increasing intensity of alteration. However, in our case, the role of oxidized meteoric water is less significant because the metasomatic rocks do not reveal a Ce anomaly. The inverse relationship of the total REE content and the degree of the Eu anomaly (Fig. 12c) indicates a substantial role of magmatogenic fluid in the formation of metasomatic rocks. Such a relationship is established in igneous rocks contrastingly to metamorphic and sedimentary rocks (Vinokurov, 1995). Metamorphic fluid is enriched in LREE with Eu and Ce anomalies (Bau, 1991; Jiang et al., 2004). The early fluid is distinguished by high REE contents and positive Eu and Ce anomalies, whereas the late fluid is depleted

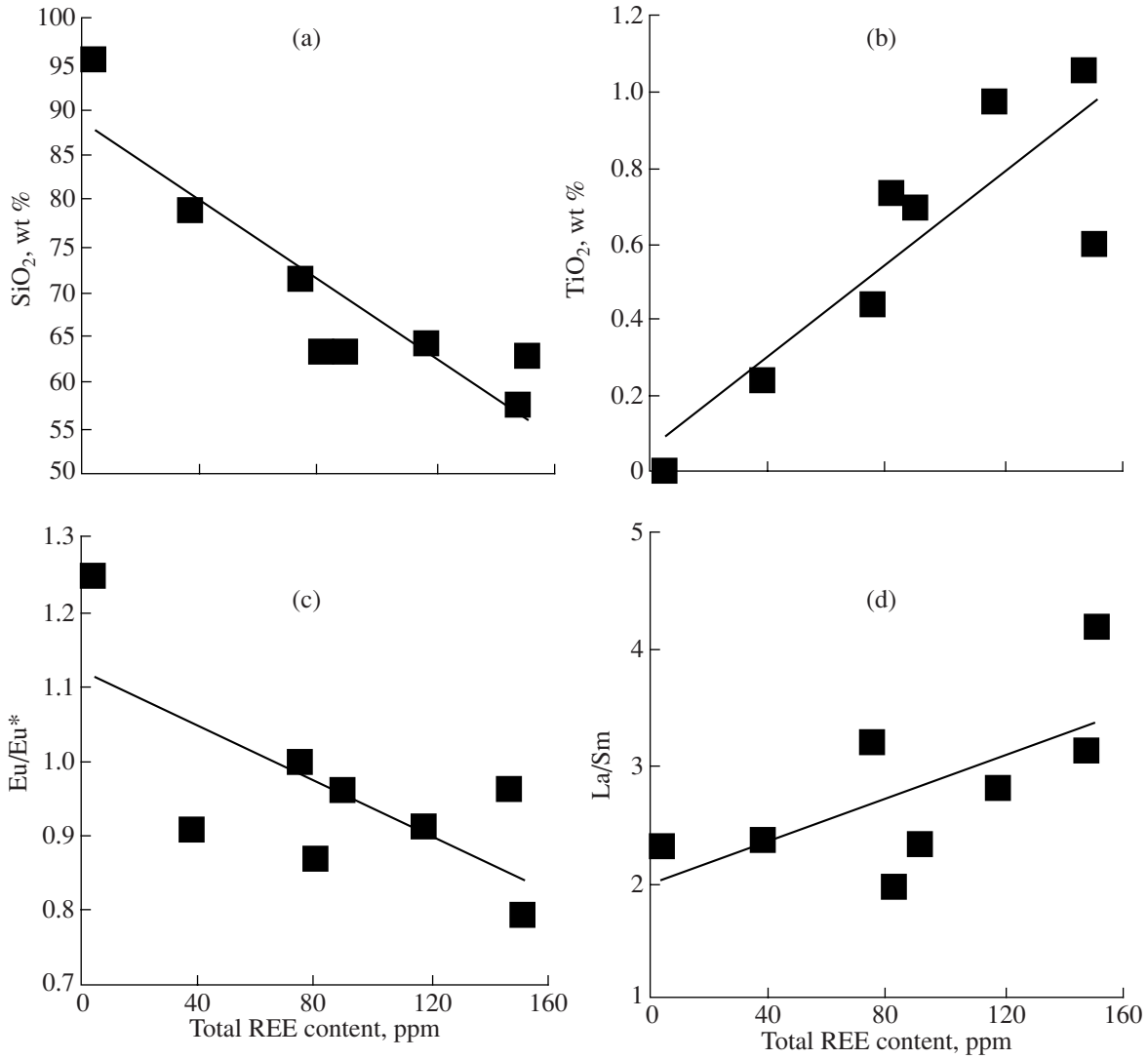

Fig. 12. Total REE content versus (a) SiO_2 and (b) TiO_2 contents and (c) Eu/Eu* and (d) La/Sm ratios in metasomatic rocks at the Natalka deposit.

in REE and Eu, and Ce anomalies become negative. The HREE contents remain practically unchanged. The REE patterns of the studied metasomatic rocks do not reveal pronounced Eu and Ce anomalies, either positive or negative (Table 9). The REE patterns of metasomatic rocks formed under decompression indicate an insignificant role of metamorphic fluid in their formation. The REE distribution in metamorphic fluid is similar to that of shale. With increasing degree of alteration and silicification, the REE pattern of metasomatic rocks markedly differs from the REE pattern of the North American Shale Composite (NASC) and sedimentary rocks in the Natalka goldfield (Fig. 12). Supposing that the composition of the outer zone of the metasomatic column is controlled by the initial rock composition, and the composition of the inner zone, by the fluid composition, the participation of metamorphic fluid in metasomatic alteration of rocks should be admitted as doubtful. Magmatic fluid is distinguished by low REE contents, and its interaction with host rocks results in dilution of the concentration and depletion of metasomatic rocks in REE.

The REE patterns of igneous rocks from the Natalka goldfield are compared in Fig. 13 with the REE patterns of metasomatic rocks formed under various conditions. The metasomatic rocks formed under decompression demonstrate the sharpest depletion in HREE, owing to their higher mobility in the hydrothermal process. The REE contents are very low in the sample enriched in vein material.

The REE patterns in igneous and sedimentary rocks are compared in Fig. 14 with REE contents in hornfels. Under conditions of contact metamorphism, hornfels undergo a redistribution of REE with insignificant depletion in LREE and enrichment in HREE.

Table 9. Parameters of REE patterns of rocks from the Natalka goldfield

Rock	Total REE, ppm	La_n/Yb_n	La_n/Sm_n	Eu_n/Eu_n^*	Ce_n/Ce_n^*
Metasomatic rocks formed under compression	71–136	6.17–12.28	1.97–4.16	0.79–0.96	1.03–1.04
Metasomatic rocks formed under decompression	4–99	6.25–18.55	2.29–3.21	0.91–1.25	0.96–1.05
Gabbrodiorite	53–183	2.54–16.5	1.31–3.54	0.99–1.04	0.91–0.99
Quartz porphyry	47–67	3.58–6.53	2.48–3.52	0.37–0.52	0.88–0.97
Siltstone	64–178	5.20–12.06	2.87–4.14	0.75–0.83	0.94–1.08
Hornfels	74–150	2.31–7.90	1.66–3.42	0.74–0.91	0.99–1.08
NASC	173	6.98	3.53	0.75	1.15

* NASC is the North American Shale Composite (Haskin et al., 1968).

The REE patterns in the studied metasomatic rocks show that all the rocks are enriched in LREE, so that participation of LREE-rich fluid in their origin is suggested. The lowest Gd_n/Yb_n ratio was established for preore beresites. This ratio rises in hydrothermally altered rocks with increasing amounts of veinlets and sulfides. The total REE concentration decreases in the same direction, owing to depletion in minerals that concentrate REE.

The Eu and Ce anomalies may be used for judging redox conditions in fluid because these elements occur in natural systems in two valence states (Bau, 1991; Ghaderi et al., 1999). At $Eu^{3+} \ll Eu^{2+}$, the minerals precipitate from a relatively reduced fluid, and at $Eu^{3+} \gg Eu^{2+}$, from a relatively oxidized fluid. As is shown in Fig. 15, the Eu/Eu* values in the studied metasomatic rocks are close to unity and clustered along the diagonal line similarly to the previously examined metasomatic rocks of the Berezovsky and Nezhdaninsky deposits (Bortnikov et al., 2007; Vikent'eva, 2007). This implies that Eu^{3+} is predominant in the metasomatic rocks formed from a relatively oxidized fluid. The elevated Eu/Eu* ratio in a sample of quartz vein may indicate a relatively reduced nature of the mineral-forming fluid (with a low Eu^{3+}/Eu^{2+} ratio).

Ce anomalies in the hydrothermally altered rocks at the Natalka deposit are not expressed; the Ce/Ce* ratio is close to unity ($0.96 < Ce/Ce^* < 1.05$) and rules out a prevalence of oxidized meteoric water in the formation of metasomatic rocks.

Thus, the study of REE patterns in the hydrothermally altered rocks at the Natalka deposit has shown that a relatively oxidized fluid enriched in LREE participated in the formation of metasomatic rocks.

As a result of REE mobility and variable stability of their complex compounds, the differentiation of HREE (Gd_n/Yb_n) increases and the differentiation of LREE (La_n/Sm_n) decreases with increasing degree of rock alteration.

The total REE content shows a negative correlation with $SiO_2$and Eu/Eu* and a positive correlation with TiO_2 and La_n/Sm_n in metasomatic rocks (Fig. 12).

In both studied sections, Eu/Eu* is inversely correlated with the degree of the tetrad effect for the third tetrad (TE_3). The correlation between TE_3 and the F content in rocks shows the important role of fluorine complexation in REE distribution (Irber et al., 1999) (Fig. 16).

The study of fluid inclusions allowed us to establish that, in the Natalka ore-forming system, minerals precipitated from three fluids different in composition: (1) a liquidlike H_2O–CO_2–NaCl–$MgCl_2$ fluid with an apparent salinity of 1.0–4.9 wt % NaCl equiv (this study) or up to 9.0 wt % NaCl equiv (Struzhkov et al., 2006); (2) a substantially gaseous mixture of CO_2 and CH_4; and (3) an aqueous salt solution with a predominance of Na and Mg chlorides with a total salinity of 7.0–5.6 wt % NaCl equiv. The first two fluids were heated up to 250–350°C under a pressure of 1.1–2.4 kbar. They existed in the mineral-forming system simultaneously and could have been formed as products of separation of the H_2O–CO_2–CH_4–NaCl–$MgCl_2$ protofluid into two immiscible liquidlike and gaseous phases.

In the opinion of many researchers, this process was the most efficient for mineral deposition, including precipitation of native gold. In low-concentration fluids, gold commonly migrates in the form of the bisulfide complex and its stability is described by the reaction

$$Au_{(cryst)} + 15/8H_2S + 1/8(SO_4)^{2-} = Au(HS)^{2-} + 1/2H_2O + 6/8H^+,$$

according to which a decrease in H_2S content due to its release into the gas phase will lower the stability of this complex (Drummond and Ohmoto, 1985).

In our view, this mechanism was not in operation during the formation of gold orebodies at the Natalka deposit because native gold is not abundant in disseminated sulfide ore.

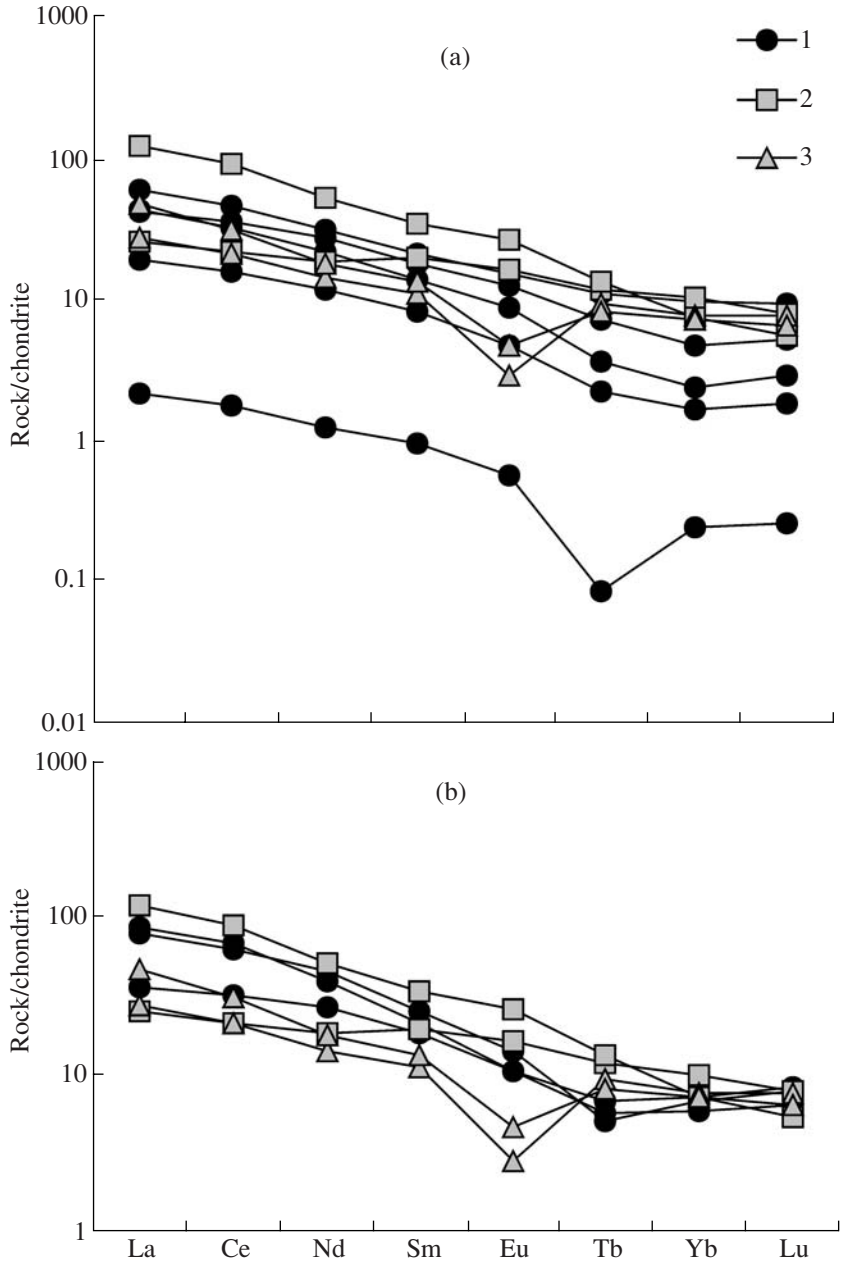

Fig. 13. Chondrite-normalized REE patterns of igneous rocks and metasomatic rocks formed under (a) decompression and (b) compression at the Natalka deposit. (1) Metasomatic rocks, (2) gabbrodiorite, (3) quartz porphyry.

Most likely, the phase separation and release of volatile components into the gas phase in the mineral-forming system of the Natalka gold deposit was a result of interaction between fluid and host rocks as a response to fluid–rock disequilibrium like at the Nezhdaninsky and Maisky deposits (Bortnikov et al., 1998, 2004). This interaction led to the metasomatic replacement of host rocks with formation of extensive halos of beresitized rocks with sulfide disseminations.

Such reactions as

$$KAl_3Si_3O_{10}(OH)_{2(Muscovite)} + 3SiO_{2(Quartz)} + 8FeAsS_{(Arsenopyrite)} + 24H_2O + 6O_2 = KFe_3AlSi_3O_{10}(OH)_{2(Biotite)} + Fe_5Al_2Si_3O_{10}(OH)_{8(Chlorite)} + 8H_3AsO_3^0 + 8H_2S^0$$

or

$$4KAl_3Si_3O_{10}(OH)_{2(Muscovite)} + 12SiO_{2(Quartz)} + 20FeAsS_{(Arsenopyrite)} + 62H_2O + 15O_2 = 4KAlSi_3O_{8(K\text{-}feldspar)} + 4Fe_5Al_2Si_3O_{10}(OH)_{8(Chlorite)} + 20H_3AsO_3^0 + 20H_2S$$

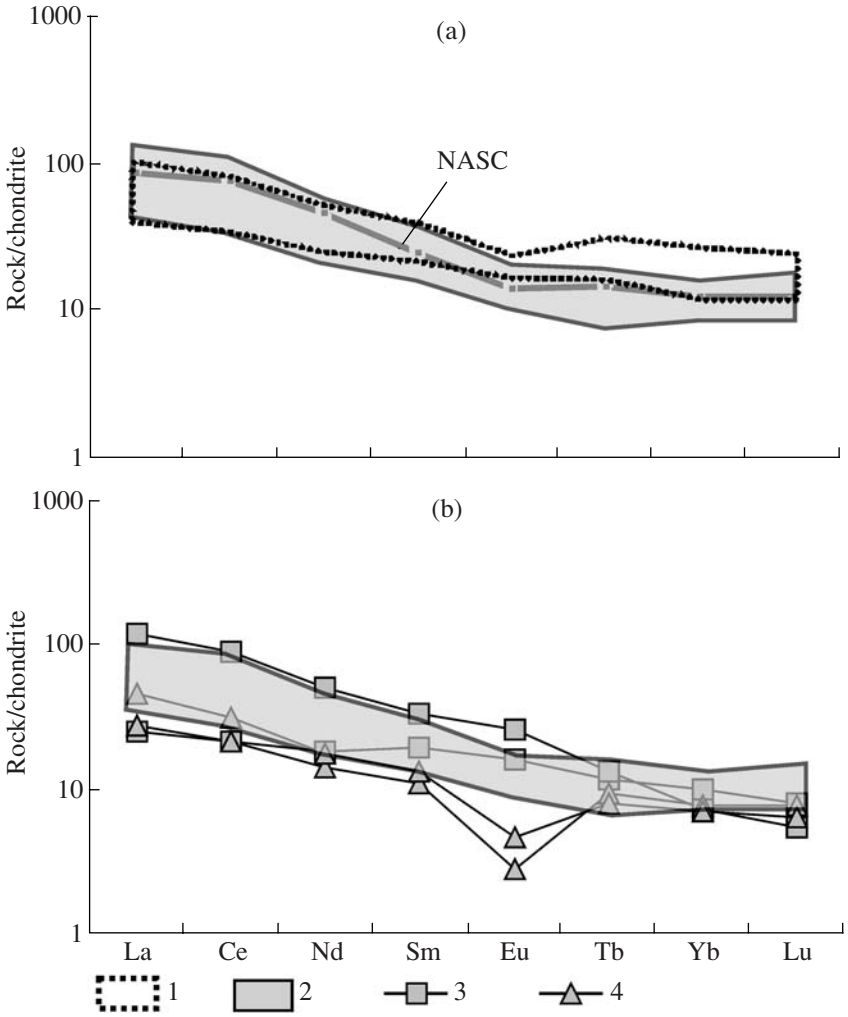

Fig. 14. Chondrite-normalized REE patterns of (a) sedimentary rocks and hornfels and (b) sedimentary and igneous rocks in the Natalka goldfield. (1) Hornfels, (2) siltstone, (3) gabbrodiorite, (4) quartz porphyry. NASC is the North American Shale Composite.

bring about the formation of arsenopyrite by sulfidation of Fe^{2+} contained in silicates of host rocks. The precipitation of considerable masses of arsenopyrite and pyrite resulted in a sharp depletion of mineral-forming fluid in hydrogen sulfide, which, in turn, led to the destabilization of the Au bisulfide complex. This metal is incorporated into arsenopyrite and to a lesser extent into pyrite as a solid solution. This point of view was stated by Goldfarb et al. (2005).

The third, medium-temperature aqueous salt fluid in the Natalka ore-forming system is suggested to be responsible for the deposition of late mineral assemblages at the final stage of ore formation. This fluid could have arisen from boiling of the H_2O–CO_2–CH_4–NaCl–$MgCl_2$ liquid, which gave rise to the metasomatic alteration of host rocks. Such a mechanism was suggested for the Charmitan gold deposit in Uzbekistan (Bortnikov et al., 1996). It is well known that precipitation of minerals leads to plugging of tectonic conduits and to a transition from hydrostatic to lithostatic pressure. Hydraulic fracturing or new tectonic movements result in crushing of the previously formed mineral aggregates. When the pressure of volatile components exceeds lithostatic loading, the lithostatic pressure is changed back to hydrostatic pressure (Hedenquist and Nenley, 1985). The pressure release decreases CO_2 solubility in the fluid, and carbon dioxide passes into the gas phase. Afterward, the volatiles migrate separately from the aqueous fluid with a high speed, leaving the aqueous fluid behind.

A late salt-bearing aqueous fluid is suggested to appear in other Au-bearing hydrothermal systems (Bortnikov, 2006). This fluid is characterized by a lower $\delta^{18}O$ of water, which serves as evidence for involvement of heated meteoric water related to a new pulse of hydrothermal activity.

Thus, the data obtained have shown that economic gold orebodies were formed as products of interaction between host rocks and a bicarbonate aqueous fluid with low to moderate salinity at a temperature of 360–

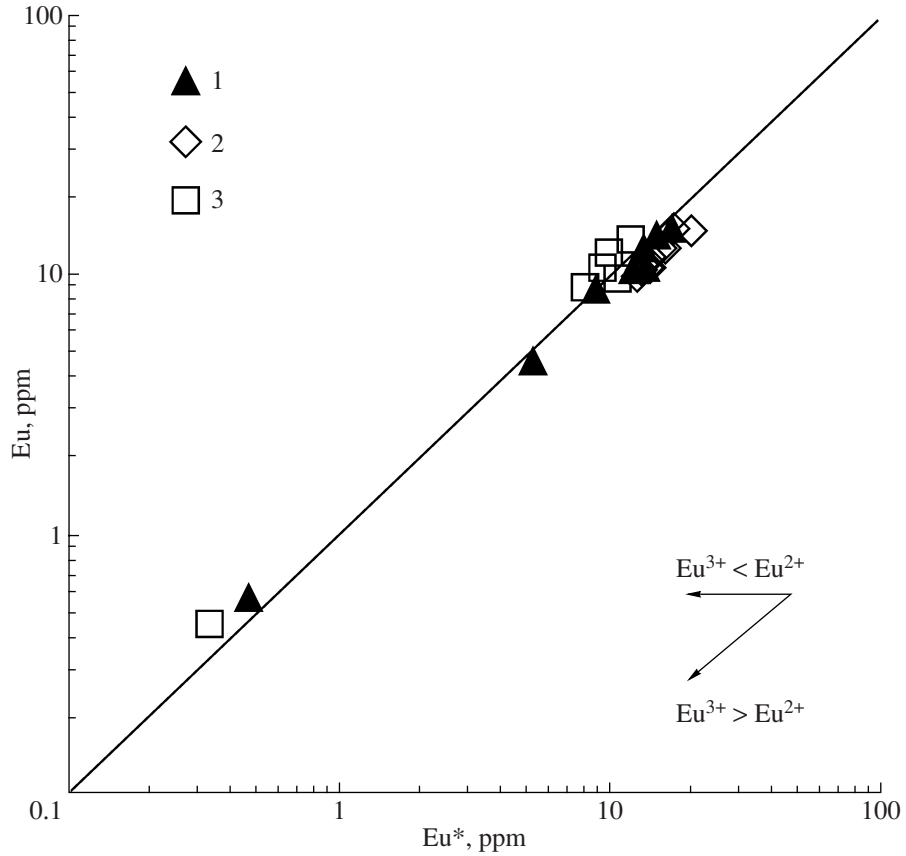

Fig. 15. Eu versus Eu* contents in the fluid coexisting with metasomatic rocks of the Natalka (1), Nezhdaninsky (2), and Berezovsky (3) gold deposits.

280°C and 1.1–2.4 kbar pressure. The salinity of ore-forming fluid at the Natalka deposit is consistent with the salinity of bicarbonate aqueous fluid (3–12 wt % NaCl equiv) established at other orogenic gold deposits (Ridley and Diamond, 2000). It should be noted that the salinity of the bicarbonate aqueous fluid is lower than that at some mesothermal gold–quartz deposits in Russia, where it attains 18 wt % NaCl equiv, but is close to the estimates reported for ore-forming fluids at the Nezhdaninsky and Maisky deposits (Bortnikov, 2006). The temperature and pressure of formation of the Natalka deposit also fall into intervals typical of mesothermal gold deposits located not only in the Yana–Kolyma Belt (Goryachev, 1992, 2003) but also in similar belts elsewhere (Bortnikov, 2006; Ridley and Diamond, 2000).

High contents of gases, in particular, methane, are noted. Methane-bearing fluid inclusions were detected in quartz at gold deposits hosted in carbonaceous terrigenous sequences (Bortnikov, 2006; Bortnikov and Prokof'ev, 2007). Some gold–quartz vein deposits in Australia are genetically related to CH_4-bearing fluids as well (Mernagh and Wygralak, 2007). The fluids enriched in methane are formed owing to reduction of CO_2. The high methane concentrations are probably caused by interaction of ore-bearing hydrothermal solutions with host carbonaceous rocks.

The oxygen isotopic composition of the parental fluid of quartz at the Natalka deposit ($\delta^{18}O_{H_2O}$ = +6.3 to +8.8‰) corresponds to the interval typical of mesothermal Au-bearing hydrothermal systems localized in metasedimentary rocks: $\delta^{18}O_{H_2O}$ = +5 to +10.0‰ (Nesbitt, 1991) or +7 to +13.0‰ (Goldfarb et al., 1991). The calculated $\delta^{18}O_{H_2O}$ = +7.6 ± 1.2‰ for the fluid in equilibrium with quartz–pyrite–arsenopyrite ore and +4.7 ± 1.1‰ for the fluid in equilibrium with minerals of the quartz–sulfide–sulfosalt assemblage suggest the supply of water from a magmatic source ($\delta^{18}O$ = +5.5 to +9.0‰). The narrow range of calculated values indicates that this source was homogeneous. An unequivocal interpretation of the origin of a fluid with such an oxygen isotopic composition is hardly possible because $\delta^{18}O$ of magmatogenic fluid and solutions that are products of dehydration of rocks as a result of regional metamorphism partly overlap.

Thus, the REE patterns of metasomatic rocks and veins at the Natalka deposit and the fluid regime of mineral formation show that this deposit has much in common in these respects with the large Nezhdaninsky

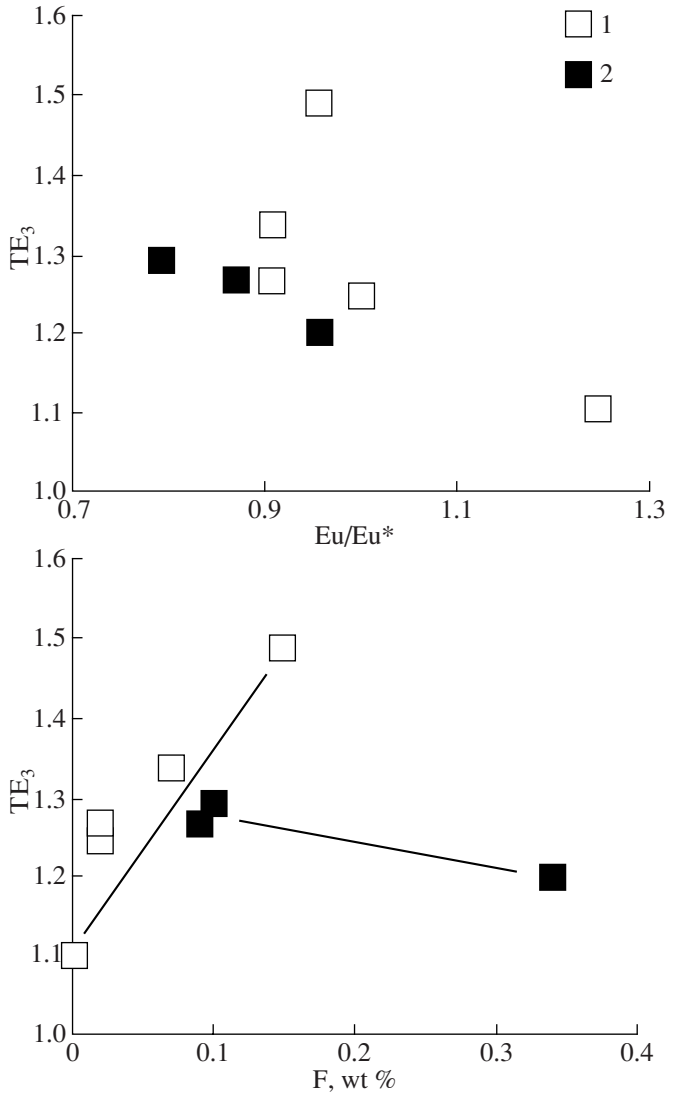

Fig. 16. Tetrad effect TE_3 versus Eu/Eu* and fluorine content in metasomatic rocks formed under (1) decompression and (2) compression at the Natalka deposit.

deposit, located in the same region. These results lead to the suggestion that large mesothermal gold deposits are close to one another in formation conditions and reduced character of ore-forming fluids of various compositions, which were involved in ore formation and supplied both magmatic components and chemical elements extracted from host rocks. In our opinion, the data obtained testify to links of ore formation with magmatic activity. Fluids separated directly from a magma chamber might have been combined with products of dehydration and decarbonation related to contact and regional metamorphism.

ACKNOWLEDGMENTS

We thank S.A. Gorbacheva, A.V. Dubinin, A.A. Avdeenko, and I.V. Grigor'eva for the performed analyses and E.E. Tyukova and A.G. Bakhareva for the samples of sedimentary and igneous rocks kindly placed at our disposal. This study was supported by the Division of Earth Sciences, Russian Academy of Sciences (fundamental research programs); the Russian Foundation for Basic Research (project nos. 05-05-64803, 06-05-64369, and 06-05-96070); the Far East Division, Russian Academy of Sciences (programs 06-I-ONZ-104 and 06-II-08-029); the International Geological Correlation Program (project IGCP 540); and the Foundation for Support of Russian Science (O.V. Vikent'eva).

REFERENCES

1. Yu. A. Balashov, *Geochemistry of Rare Earth Elements* (Nauka, Moscow, 1976) [in Russian].
2. M. Bau and P. Möller, "Rare Earth Elements Fractionation in Metamorphogenic Hydrothermal Calcite, Magnesite and Siderite," Mineral. Petrol. **45**, 231–246 (1992).
3. F. P. Bierlein and S. Maher, "Orogenic Disseminated Gold in Phanerozoic Fold Belts: Examples from Victoria, Australia and Elsewhere," Ore Geol. Rev. **17**, 215–232 (2001).
4. R. J. Bodnar and M. O. Vityk, "Interpretation of Microthermometric Data for H_2O–NaCl Fluid Inclusions," in *Fluid Inclusions in Minerals: Methods and Applications* (Siena, Pontignano, 1994), pp. 117–130.
5. A. S. Borisenko, "Study of Salt Composition of Fluid Inclusions in Minerals with Cryometric Method," Geol. Geofiz. **18** (8), 16–27 (1977).
6. N. S. Bortnikov, "Mineralogy, Geochemistry and Origin of the Black Shale Hosted Gold Deposits of the Former Soviet Union," in *Mineral Deposits: from Their Origin to Their Environmental Impacts* (Prague, 1995), pp. 935–937.
7. N. S. Bortnikov, "Geochemistry and Genesis of the Ore-Forming Fluids in Hydrothermal–Magmatic Systems in Tectonically Active Zones," Geol. Rudn. Mestorozhd. **48** (1), 3–28 (2006) [Geol. Ore Deposits **48** (1), 1–22 (2006)].
8. N. S. Bortnikov and V. Y. Prokof'ev, "World-Class Mesothermal Gold Deposits of Russia: Composition and Origin of Ore-Forming Fluids," in *Proceedings of the 9th Biennial SGA Meeting on Mineral Exploration and Research: Digging Deeper* (Dublin, 2007), Vol. 1, pp. 793–796.
9. N. S. Bortnikov, G. N. Gamyanin, O. V. Vikent'eva, et al., "Fluid Composition and Origin in the Hydrothermal System of the Nezhdaninsky Gold Deposit, Sakha (Yakutia), Russia," Geol. Rudn. Mestorozhd. **49** (2), 99–145 (2007) [Geol. Ore Deposits **49** (2), 87–128 (2007)].
10. N. S. Bortnikov, G. N. Gamyanin, V. B. Naumov, and L. P. Nosik, "The Nezhdaninskoye Mesothermal Gold Deposit, Russia: Ore-Forming Fluid and Deposition Environment," in *Current Research in Geology Applied to Ore Deposits* (Univ. Granada, Granada, 1993), pp. 419–422.
11. N. S. Bortnikov, G. N. Gamyanin, V. V. Alpatov, et al., "Mineralogy, Geochemistry, and Origin of the Nezhdan-

insky Gold Deposit (Sakha-Yakutia, Russia)," Geol. Rudn. Mestorozhd. **40** (2), 137–156 (1998) [Geol. Ore Deposits **40** (2), 121–138 (1998)].

12. N. S. Bortnikov, I. A. Bryzgalov, N. N. Krivitskaya, et al., "The Maisky Multistage Stringer–Disseminated Gold–Sulfide Deposit (Chukotka, Russia): Mineralogy, Fluid Inclusions, Stable Isotopes (O and S), History, and Formation Conditions," Geol. Rudn. Mestorozhd. **46** (6), 475–509 (2004) [Geol. Ore Deposits **46** (6), 409–440 (2004)].
13. N. S. Bortnikov, V. N. Sazonov, I. V. Vikentyev, et al., "The Berezovsky Giant Gold Quartz Deposit, Urals, Russia: Fluid Inclusion and Stable Isotope Studies," in *Mineral Deposits: Research and Exploration—Where Do They Meet?* (Balkema, Rotterdam, 1997), pp. 157–160.
14. N. S. Bortnikov, V. Yu. Prokof'ev, and N. V. Razdolina, "Origin of the Charmitan Gold–Quartz Deposit (Uzbekistan)," Geol. Rudn. Mestorozhd. **38** (3), 238–257 (1996) [Geol. Ore Deposits **38** (3), 208–226 (1996)].
15. P. Brown, "FLINCOR: a Computer Program for the Reduction and Investigation of Fluid Inclusion Data," Am. Mineral. **74**, 1390–1393 (1989).
16. V. A. Buryak, I. S. Nemenman, N. V. Berdnikov, et al., "Fluid Regime of Formation and Source of Ore-Forming Solutions of Gold–Quartz Lodes in the Allakh-Yun Zone," Tikhookean. Geol. **9** (3), 62–70 (1990).
17. G. M. Claypool and J. R. Kaplan, "The Origin and Distribution of Methane in Marine Sediments," in *Natural Gases in Marine Sediments* (Plenum Press, New York, 1974), Vol. 3, p. 132.
18. P. L. P. Collins, "Gas Hydrates in CO_2-Bearing Fluid Inclusions and the Use of Freezing Data for Estimation of Salinity," Econ. Geol. **74**, 1435–1444 (1979).
19. R. S. Darling, "An Extended Equation to Calculate NaCl Contents from Final Clathrate Melting Temperatures in H_2O–CO_2–NaCl Fluid Inclusions: Implications for P–T–Isochors Location," Geochim. Cosmochim. Acta **55**, 3869–3871 (1991).
20. S. E. Drummond and H. Ohmoto, "Chemical Evolution and Mineral Deposition in Boiling Hydrothermal Systems," Econ. Geol. **89**, 126–147 (1985).
21. R. A. Eremin, S. V. Voroshin, V. A. Sidorov, et al., "Geology and Genesis of the Natalka Gold Deposit, Northeast Russia," Int. Geol. Review **36**, 1113–1138 (1994).
22. L. V. Firsov, "Age of Spessarite–Vogesite with Quartz Fragments at the Natalka Deposit," Kolyma, No. 10, 34–37 (1964).
23. L. V. Firsov, "K–Ar Dating of Pre- and Postmineral Dikes in the Yana–Kolyma Gold Belt," Izv. Akad. Nauk SSSR, Ser. Geol., No. 11, 204–210 (1967).
24. G. N. Gamyanin, N. S. Bortnikov, and V. V. Alpatov, *The Nezhdaninsky Gold Deposit: An Unique Deposit of Northeastern Russia* (Geos, Moscow, 2000) [in Russian].
25. *Geodynamics, Magmatism, and Metallogeny of the Russian Far East* (Dal'nauka, Vladivostok, 2006) [in Russian].
26. M. Ghaderi, M. Palin, I. H. Campbell, and P. J. Sylvester, "Rare Earth Element Systematics in Scheelite from Hydrothermal Gold Deposits in the Kalgoorlie–Norseman Region, Western Australia," Econ. Geol. **94**, 423–438 (1999).
27. R. J. Goldfarb, N. Baker, and B. Dube, "Distribution, Character and Genesis of Gold Deposits in Metamorphic Terranes," Econ. Geol. **100**, 407–409 (2005).
28. R. J. Goldfarb, D. L. Leach, S. C. Rose, and G. P. Landis, "Fluid Inclusion Geochemistry of Gold-Bearing Quartz Veins of the Juneau Gold Belt, Southeastern Alaska: Implications for Ore Genesis," Econ. Geol. Monograph **6**, 363–375 (1989).
29. R. J. Goldfarb, R. J. Newberry, W. J. Pickthhorn, and C. L. Gent, "Oxygen, Hydrogen and Sulfur Isotope Studies in the Juneau Gold Belt, Southeastern Alaska: Constraints on the Origin of Hydrothermal Fluids," Econ. Geol. **86**, 66–80 (1991).
30. V. V. Golub and N. A. Goryachev, "Role of Transverse Faults in Localization of Gold Mineralization of the Natalka Deposit," in *Proceedings of All-Russian Conference: Science of Northeastern Russia—the Onset of Century* (SVKNII, Magadan, 2005), pp. 158–160 [in Russian].
31. V. V. Golub and N. A. Goryachev, *Mineralogical and Geochemical Features of Ore Zones and Ore Shoots at Deep Levels of the Natalka Deposit* (Yakutian Sci. Center, Siberian Branch, Russian Acad. Sci., Yakutsk, 2006) [in Russian].
32. S. Yu. Golubev, "Morphology of Orebodies at the Natalka Gold–Quartz Large-Tonnage Deposit," in *Proceedings of Scientific and Practical Conference on Forecasting, Exploration, and Evaluation of Metallic and Nonmetallic Deposits: Advances and Outlook* (TsNIGRI, Moscow, 2008), p. 58.
33. V. I. Goncharov, S. V. Voroshin, and V. A. Sidorov, *The Natalka Gold Deposit* (Severovost. Nauchn. Tsentr Dalnevost. Otd. Ross. Akad. Nauk, Magadan, 2002) [in Russian].
34. N. A. Goryachev, *Veined Quartz of Gold Deposits in the Yano-Kolyma Belt* (SVKNII, Magadan, 1992) [in Russian].
35. N. A. Goryachev, *Genesis of Gold–Quartz Vein Belts of the North Pacific* (SVKNII, Magadan, 2003) [in Russian].
36. N. A. Goryachev, V. A. Sidorov, I. S. Litvinenko, and T. I. Mikhalitsyna, "Mineral Composition, Petrographic, and Geochemical Features of Ore Zones at Deep Levels of the Natalka Deposit," Kolyma, No. 2, 38–49 (2000).
37. S. A. Grigorov, "Genesis and Formation Dynamics of the Natalka Gold Deposit As Deduced from Systematic Analysis of Geochemical Field," Rudy Met., No. 3, 44–48 (2006).
38. D. I. Groves, R. J. Goldfarb, F. Robert, and C. J. R. Hart, "Gold Deposits in Metamorphic Belts: Overview of Current Understanding, Outstanding Problems, Future Research, and Exploration Significance," Econ. Geol. **98**, 1–29 (2003).
39. L. A. Haskin, M. A. Haskin, F. A. Frey, and T. R. Wildman, "Relative and Absolute Terrestrial Abundances of the Rare Earths," in *Origin and Distribution of the Elements* (Pergamon, New York, 1968), pp. 889–912.
40. J. W. Hedenquist and R. W. Henley, "The importance of CO_2 on Freezing Point Measurements of Fluid Inclusions: Evidence from Active Geothermal Systems and Implications for Epithermal Ore Deposition," Econ. Geol. **80**, 1379–1406 (1985).

41. C. J. Hodgson, D. A. Love, and J. V. Hamilton, "Giant Mesothermal Gold Deposits: Descriptive Characteristics, Genetic Model and Exploration Are Selection Criteria," in *Giant Ore Deposits. SEG SP-2* (1993), pp. 157–206.
42. W. Irber, "The Lanthanide Tetrad Effect and Its Correlation with K/Rb, Eu/Eu*, Sr/Eu, Y/Ho, and Zr/Hf of Evolving Peraluminous Granite Suites," Geochim. Cosmochim. Acta **63** (3/4), 489–508 (1999).
43. S.-Y. Jiang, J.-M. Yu, and J.-J. Lu, "Trace and Rare-Earth Element Geochemistry in Tourmaline and Cassiterite from the Yunlong Tin Deposit, Yunnan, China: Implication for Magmatitic–Hydrothermal Fluid Evolution and Ore Genesis," Chem. Geol. **209**, 193–213 (2004).
44. A. I. Kalinin, *Multifactor Forecasting and Exploration Models of Gold and Silver Deposits in Northeastern Russia* (Nedra, Moscow, 1992) [in Russian].
45. A. I. Kalinin, V. K. Kanishchev, A. G. Orlov, and V. V. Gashtol'd, "Structure of the Natalka Ore Field," Kolyma, No. 10/11, 10–14 (1992).
46. V. A. Kalyuzhny, *Principles of the Science on Mineral-Forming Fluids* (Naukova Dumka, Kiev, 1982) [in Russian].
47. R. Kerrich, "Mesothermal Gold Deposits: A Critique of Genetic Hypotheses," in *Greenstone Gold and Crustal Evolution* (Geol. Assoc. Canada, 1990), pp. 13–31.
48. R. Kerrich, R. J. Goldfarb, D. I. Groves, and S. Garwin, "The Geodynamics of World-Class Gold Deposits: Characteristics, Space-Time Distribution and Origins," Rev. Econ. Geol. **13**, 501–551 (2000).
49. I. M. Khasanov, V. G. Ermolenko, and V. G. Shakhtyrov, "Deep Structure of the Omchak Ore Cluster," in *Problems of Geology and Metallogeny of Northeastern Asia at the Turn of Millenniums* (SVKNII, Magadan, 2001), Vol. 1, pp. 286–289 [in Russian].
50. M. M. Konstantinov, E. M. Nekrasov, A. A. Sidorov, and S. F. Struzhkov, *Gold Giants of Russia and the World* (Nauchnyi Mir, Moscow, 2000) [in Russian].
51. O. P. Kreuzer, "Intrusion-Hosted Mineralization in the Charters Towers Goldfield, North Queensland: New Isotopic and Fluid Inclusion Constraints on the Timing and Origin of the Auriferous Veins," Econ. Geol. **100**, 1583–1603 (2005).
52. N. K. Kurbanov, Ch. Kh. Arifulov, P. G. Kucherevsky, et al., "Geological and Genetic Models of the Gold Deposits in Carbonaceous Terrigenous Complexes," Rudy Met., No. 2, 55–69 (1994).
53. V. G. Lashkov, E. L. Bel'chenko, and B. V. Guzman, *Gold of Russia's Subsurface* (EKOS, Moscow, 2000) [in Russian].
54. B. G. Lottermoser, "Rare Earth Elements and Hydrothermal Ore Formation Processes," Ore Geol. Rev. **7**, 25–41 (1992).
55. Y. Matsuhisa, J. R. Goldsmith, and R. N. Clayton, "Oxygen Isotopic Fractionation in the System Quartz–Albite–Anorthite–Water," Geochim. Cosmochim. Acta **43**, 1131–1140 (1979).
56. *Metasomatism and Metasomatic Rocks* (Nauchnyi Mir, Moscow, 1998) [in Russian].
57. S. V. Mezhov, "Geological Structure of the Natalka Gold Deposit," Kolymskie Vesti, No. 9, 8–17 (2000).
58. S. V. Mezhov and I. M. Khasanov, "Deep Structure of the Southwestern Limb of the Ayan-Yuryakh Anticlinorium," in *Geology and Metallogeny of the Northeastern Asia at the Turn of Milleniums* (SVKNII, Magadan, 2001), Vol. 1, pp. 263–266 [in Russian].
59. R. M. Mirgorodskaya, E. A. Zimenko, N. A. Goryachev, et al., "Molybdenum Porphyry Mineralization of the Omchak Ore Cluster," in *Geology, Geography, and Biological Diversity of Northeastern Russia* (SVKNII, Magadan, 2006), pp. 162–163 [in Russian].
60. B. E. Nesbitt, "Phanerozoic Gold Deposits in Tectonically Active Continental Margins," in *Gold Metallogeny and Exploration* (Blackie and Son, Glasgow, 1991), pp. 104–132.
61. B. E. Nesbitt and K. Muchlenbachs, "Geology, Geochemistry, and Genesis of Mesothermal Lode Gold Deposits of the Canadian Cordillera: Evidence for Ore Formation from Evolved Meteoric Water," Econ. Geol. Monograph **6**, 553–563 (1989).
62. R. J. Newberry, P. W. Layer, P. B. Hans, et al., "Prelimenery Analysis of Chronology of Mesozoic Magmatism, Tectonics, and Ore Mineralization in Northeastern Russia: $^{40}Ar/^{39}Ar$ Dating and Trace Elements of Igneous and Ore-Bearing Rocks," in *Gold Mineralization and Granitoid Magmatism of the Northern Pacific: Vol. 1., Geology, Geochronology, and Geochemistry* (SVKNII, Magadan, 2000), pp. 181–205 [in Russian].
63. V. A. Pristavko, V. A. Sidorov, T. I. Mikhalitsina, et al., "Geological and Geochemical Model of the Natalka Gold Deposit," Kolymskie Vesti, No. 9, 18–24 (2000).
64. J. R. Ridley and L. W. Diamond, "Fluid Chemistry of Orogenic Lode Gold Deposits and Implication for Genetic Models. Gold in 2000," Rev. Econ. Geol **13**, 141–162 (2000).
65. E. Roedder, *Fluid Inclusions in Minerals* (Reviews in Mineralogy, Mineral. Soc. Amer., 1984, Vol. 12; Mir, Moscow, 1987).
66. V. N. Sazonov, O. V. Vikent'eva, V. N. Ogorodnikov, et al., "REE in Columns of Propylitization, Albitization, Aceitization, and Beresitization–Listvenitization of Rocks with Various Silica Content: Evolution of Distribution, Causes, and Practical Implications," Litosfera, No. 3, 108–124 (2006).
67. V. M. Sharafutdinov and I. M. Khasanov, "Petrophysical Zoning of the Natalka Gold Deposit," Vestn. Severovost. Nauchn. Tsentr, Dal'nevost. Otd. Ross. Akad. Nauk, No. 4, 2–11 (2006).
68. A. A. Sidorov and I. N. Tomson, "Ore Potential of Black Shale Sequences: Convergence of Alternative Concepts," Vestn. Ross. Akad. Nauk **70** (8), 719–724 (2000).
69. A. A. Sidorov, N. A. Goryachev, N. E. Savva, et al., *Essays on Metallogeny and Geology of Ore Deposits in Northeastern Russia* (Severovost. Nauchn. Tsentr, Dal'nevost. Otd. Ross. Akad. Nauk, Magadan, 1994) [in Russian].
70. V. A. Sidorov, N. A. Goryachev, and E. A. Zimenko, "The Cretaceous Volcanic Vent of the Vanin Stock (Omchak Ore Cluster): An Unique Geological Monument," in *Geodynamics, Magmatism, and Minerageny of the North Pacific Continental Margins* (SVKNII, Magadan, 2003), Vol. 2, pp. 149–153 [in Russian].

71. V. A. Stepanov, *Zoning of Gold–Quartz Mineralization in the Central Kolyma (Magadan oblast, Russia)* (Dal'nauka, Vladivostok, 2001), pp. 42–51 [in Russian].

72. S. F. Struzhkov, M. V. Natalenko, V. B. Chekvaidze, et al., "A Multifactor Model of the Natalka Gold Deposit," Rudy Met., No. 3, 34–44 (2006).

73. R. T. Taylor and B. J. Fryer, "Rare Earth Element Chemistry As an Aid to Interpretating Hydrothermal Ore Deposits," in *Metallization Associated with Acid Magmatism* (Wiley, New York, 1982), Vol. 6, pp. 357–365.

74. R. Thiery, A. M. Kerkhof, and J. Dubessy, "VX Properties of CH_4–CO_2 and CO_2–N_2 Fluid Inclusions: Modeling for $T < 31°C$ and $P < 400$ Bars," Eur. J. Mineral. **6**, 753–771 (1994).

75. E. E. Tyukova and S. V. Voroshin, *Composition and Parageneses of Arsenopyrite in Deposits and Host Rocks of the Upper Kolyma Region (to Interpretation of Genesis of Sulfide Asssemblages)* (Severovost. Nauchn. Tsentr Dalnevost. Otd. Ross. Akad. Nauk, Magadan, 2007) [in Russian].

76. E. E. Tyukova, T. I. Mikhalitsyna, and O. V. Vikent'eva, "Rare Earth Mineralization of the Natalka Gold Deposit (Magadan oblast)," in *Geochemistry and Ore Formation of Radioactive, Noble, and Rare Metals in Endogenic and Exogenic Processes* (Ulan-Ude, 2007), pp. 168–171.

77. O. V. Vikent'eva, "REE in Metasomatic Rocks of Mesothermal Gold Deposits," in *Proceedings of Annual Session of Russian Mineralogical Society Dedicated to the 110th Anniversary of Academician A.G. Betekhtin (1897–2007) on Role of Mineralogy in Knowledge of Ore Formation* (IGEM RAS, Moscow, 2007), pp. 76–80.

78. S. F. Vinokurov, "Geochemical Significance of Europium Anomalies in the Minerals of Ore Deposits," Geochem. Int. **32** (12), 113–140 (1995).

79. S. V. Voroshin, V. G. Shakhtyrov, and E. E. Tyukova, "Geology and Genesis of the Natalka Gold Deposit," Kolyma, No. 2, 22–31 (2000).